


RESEARCH

Open Access



# Development of an oligosaccharide library to characterise the structural variation in glucuronoarabinoxylan in the cell walls of vegetative tissues in grasses

Theodora Tryfona<sup>1</sup>, Mathias Sorieul<sup>1,3</sup>, Carolina Feijao<sup>1,4</sup>, Katherine Stott<sup>2</sup>, Denis V. Rubtsov<sup>1,5</sup>, Nadine Anders<sup>1</sup> and Paul Dupree<sup>1\*</sup> 

## Abstract

**Background:** Grass glucuronoarabinoxylan (GAX) substitutions can inhibit enzymatic degradation and are involved in the interaction of xylan with cell wall cellulose and lignin, factors which contribute to the recalcitrance of biomass to saccharification. Therefore, identification of xylan characteristics central to biomass biorefining improvement is essential. However, the task of assessing biomass quality is complicated and is often hindered by the lack of a reference for a given crop.

**Results:** In this study, we created a reference library, expressed in glucose units, of *Miscanthus sinensis* GAX stem and leaf oligosaccharides, using DNA sequencer-Assisted Saccharide analysis in high throughput (DASH), supported by liquid chromatography (LC), nuclear magnetic resonance (NMR) spectroscopy and mass spectrometry (MS). Our analysis of a number of grass species highlighted variations in substitution type and frequency of stem and leaf GAX. In miscanthus, for example, the  $\beta$ -Xylp-(1  $\rightarrow$  2)- $\alpha$ -Araf-(1  $\rightarrow$  3) side chain is more abundant in leaf than stem.

**Conclusions:** The reference library allows fast identification and comparison of GAX structures from different plants and tissues. Ultimately, this reference library can be used in directing biomass selection and improving biorefining.

**Keywords:** Grass xylan, Bioenergy, Tissue variation, Species variation, Xylan branching, DASH

## Background

Plant xylan polysaccharides have attracted attention due to their numerous applications not only in the papermaking, baking and food industries but also in respect to bioenergy production. Branched xylan is the main hemicellulose in many crops. This xylan is made of a linear chain of  $\beta$ -(1  $\rightarrow$  4)-linked xylopyranosyl (Xylp) residues, which can be substituted by  $\alpha$ -(1  $\rightarrow$  2)-linked (4-O-methyl-)glucuronic acid ([Me]GlcA) and acetylation at the O-2 and/or O-3 positions [1]. In monocots, such as grasses, and also in gymnosperms, xylan

is additionally modified by  $\alpha$ -(1  $\rightarrow$  3)-linked L-arabinofuranosyl residues (Araf). The Araf residues may be further substituted at O-2 with an Araf or a Xylp residue [2]. Cereal grain endosperm contains neutral arabinoxylan (AX), which is monosubstituted with  $\alpha$ -(1  $\rightarrow$  3)-linked Araf residues or di-substituted with  $\alpha$ -(1  $\rightarrow$  2)-linked and  $\alpha$ -(1  $\rightarrow$  3)-linked Araf residues [1, 3]. Araf residues of both glucuronoarabinoxylan (GAX) and endosperm AX may be esterified with a feruloyl (Fer)- or coumaryl group at O-5 position [4, 5]. Feruloylation has been implicated in cross-linking of different xylan chains and in cross-linking to lignin [6, 7]. Feruloylated Araf structures can be further substituted with  $\beta$ -(1  $\rightarrow$  2)-linked Xylp groups or additional sugars [8, 9]. Corn bran xylan was found to contain  $\alpha$ -(1  $\rightarrow$  2)-linked L-Galp on the Xylp residue of the

\*Correspondence: pd101@cam.ac.uk

<sup>1</sup> Department of Biochemistry, University of Cambridge, Hopkins Building, The Downing Site, Tennis Court Road, Cambridge CB2 1QW, UK  
Full list of author information is available at the end of the article



Fer-Araf-Xylp oligomeric structure [10–12], and this was recently found to be present in other cereal grains as well [13, 14]. Among the ferulate-containing xylan side-chain variants, 5-O-Fer-Araf structure appears most abundant, followed by the Xylp-[5-O-Fer]-Araf structure [8]. Grass GAX and AX is acetylated but to a lesser extent than dicot glucuronoxylan. However, in addition to acetyl groups being added to the backbone Xylp residues, the Araf substituents can carry acetyl groups at O-2 [15].

Most of the energy in the lignocellulosic biomass is locked within the secondary cell walls in the form of cellulose and xylan, which form a dense matrix with lignin [16]. Lignocellulosic plant cell wall recalcitrance is a barrier to cost-effective cellulosic biofuel production. Cell wall recalcitrance in regards to xylan is influenced by various factors: heavy substitution of xylan, which can impair the action of hydrolytic enzymes; specific branching points, which can serve as cross-linking sites with lignin and the pattern of branching, which can affect the interaction of xylan with cellulose [17]. The importance of xylan in recalcitrance is illustrated by the finding that removal of xylan in switchgrass resulted in materials that achieved nearly 100% glucose yields in subsequent enzymatic hydrolysis [18].

In order to improve the biomass of bioenergy crops and optimise the biorefining processes, information on the structure of xylan, and its variation, is crucial. However, little is known about the variability of xylan structure of grasses in, e.g. different tissues like stems and leaves. In addition, analysis methods of xylooligosaccharides have to be fast, accurate and robust. The majority of detailed structural information on xylan in grasses is based on analysis of cereal grain xylans such as corn cob, oat spelt, barley husks or wheat endosperm often using LC, NMR and MS [19–23]. More recently, structures of xylan of lignified tissues were analysed in grasses [24–26]. Oligosaccharides with different degrees of polymerisation (DP), glycosidic linkages and saccharide composition can be resolved with DNA sequencer-Assisted Saccharide analysis High throughput (DASH) which can analyse simultaneously 96 samples by capillary electrophoresis [27]. Our study provides the detailed structural characterisation of xylan oligosaccharides from *Miscanthus sinensis* stem cell walls hydrolysed with xylan-specific glycosyl hydrolases (GH) from the families 10 and 11. This information was used to generate a DASH reference library of GAX oligosaccharides with their corresponding glucose units (GU) as mobility standards. This library allows the fast and quantitative comparison of GAX oligosaccharide structures using the high-throughput method DASH, as shown by the comparison of oligosaccharide profiles of leaf and grass GAX from different grasses. Relative

quantification of side chains can be achieved as exemplified by the more detailed analysis of miscanthus stem and leaf GAX.

## Results

### Development of a GAX oligosaccharide library from *Miscanthus sinensis* stem

In order to use DASH as a high-throughput method to characterise GAX structures and achieve relative quantification of different xylan substitutions, a GAX oligosaccharide library had to be created to serve as a standard for structural analysis. To develop this library, *Miscanthus sinensis* stem GAX was hydrolysed with endo- $\beta$ -xylanases GH10 and GH11, respectively. Most reported xylanases classify into these two families, which are described to have slightly different substrate specificities. Briefly, GH10 xylanases are more capable of hydrolysing adjacent to substitutions of the xylan backbone, while GH11 xylanases preferably act on relatively unsubstituted parts of xylan [28, 29].

To describe the various hydrolysis products we use the heteroxylan naming system suggested by Faure et al. [30] with the exception of xylooligosaccharide standards which are described as X<sub>1</sub>–X<sub>6</sub> corresponding to xylose, xylobiose, xylotriose, xylotetraose, xylopentaose and xylohexaose.

The DASH capillary electropherograms were first aligned using the internal mobility migration markers mixed with each sample to eliminate variation between capillaries [27]. The GAX oligosaccharide library was compiled by assigning the characterised oligosaccharide structures to DASH peaks based on their migration in DASH. The migration of the oligosaccharides was compared to the migration of dextran standards to provide migration information in a method we adapted here from liquid chromatography [31]. By providing the migration of the xylooligosaccharides in GU, the identification is more robust to any changes in capillary sequencer variation. Comparison of oligosaccharide GU migration therefore allows the fast and reliable annotation of GAX structures in unknown samples to all DASH users.

To characterise the detailed structure of GAX oligosaccharides, we separated the hydrolysis products by SEC and all fractions were analysed by DASH. Based on the result of the DASH analysis, SEC fractions were selected in which the respective oligosaccharides were highly abundant. Part of these fractions was subjected to secondary enzymatic hydrolysis followed by DASH analysis. The other part was used to separate possible structural isomers by Hydrophilic Interactions Liquid Chromatography (HILIC) followed by off-line Matrix-Assisted laser Desorption Ionisation (MALDI)-Mass Spectrometry. The oligosaccharides were then subjected

to high-energy MALDI Collision-Induced Dissociation (CID) for detailed structural analysis. Ultimately, DASH peaks were matched to oligosaccharide structures characterised with HILIC–MALDI–MS/MS CID by combining data on peak abundance and enzyme sensitivity from different SEC fractions.

Based on the previously characterised composition of grass GAX [1], in the MALDI-CID spectra we assign uronic acid substitutions as GlcA and furanosyl pentosyl substitutions as Araf on a 1,4-linked Xylp backbone. Given that no GlcA residues on xylan have been reported to carry a methyl modification on the O-6, we assign methyl group modifications at O-4. In addition, all oligosaccharides characterised here are generated by GH10 or GH11 endo- $\beta$ -1,4 xylanases and therefore the non-reducing end backbone Xylp residues cannot be modified at the O-4. Glycosidic bond and cross-ring product ions are labelled according to the nomenclature of Domon and Costello [32]. The D, E, G and V ions are labelled according to previously established nomenclature [33–35]. We used sequential digests of the oligosaccharides with enzymes to gain further insights into the structure and to confirm the results of the MALDI-CID: arabinofuranosidases GH51 and GH62 hydrolyse single Araf substitutions but not Xylp [36], which helps to distinguish the nature of pentosyl side chains; glucuronidases GH67 and GH115 both remove [Me]GlcA substitutions. However, GH67 can only remove terminal GlcA from the non-reducing end, whereas GH115 preferably acts on substitutions of internal regions although it will also cleave GlcA from non-reducing terminal Xylp residues albeit at a slower rate [37, 38].

An overview of the analysis is depicted in Fig. 1.

#### GAX oligosaccharide profiles of xylanase GH10 and GH11 hydrolysis of *Miscanthus sinensis*

In brief, a standard DASH profile was generated by APTS labelling of GH10 and GH11 hydrolysis products of *Miscanthus sinensis* stem alcohol-insoluble residue (AIR), respectively, and analysis by DASH (Fig. 2).

In order to partially separate the oligosaccharides for further structural analysis, the hydrolysis products were subjected to Size Exclusion Chromatography (SEC). Eighty *Miscanthus sinensis* GH10 and GH11 oligosaccharide SEC fractions (*Ms10\_1–80* and *Ms11\_1–80*) were collected and labelled with APTS and analysed by DASH, revealing separation of a number of oligosaccharides by SEC (Fig. 3 and Additional file 1: Figure S1) in comparison to the standard DASH profile prior to SEC (Fig. 2). Figure 3 and Additional file 1: Figure S1 also show the power of DASH to study a large number of oligosaccharide mixtures, to aid interpretation of the SEC separation and selection of fractions of interest.

Some oligosaccharides separated by DASH eluted at the same time as  $\beta$ -(1 $\rightarrow$ 4)-xylooligosaccharide ( $X_1$ – $X_6$ ) standards; other oligosaccharides (namely  $XU^2XX$ ,  $XU^{(4Me)2}XX$  and  $XA^3XX$ ) were previously structurally characterised [27–29]. The identity of their DASH peaks was confirmed by MALDI-CID (data not shown). Remaining unknown peaks were labelled  $N_{1-12}$  (Fig. 2). The detailed results of the structural analysis of each oligosaccharide are described below. Table 1 summarises the GAX oligosaccharide structures generated by GH10 and GH11 hydrolysis and their corresponding GU. Table 2 summarises the sensitivity/resistance to enzymatic hydrolysis of GAX oligosaccharides and Additional file 1: Figure S2 shows the sensitivity/resistance of selected oligosaccharides to enzymatic hydrolysis.

#### Structural characterisation of the oligosaccharides $N_1$ – $N_9$ from the xylanase GH10 digest of *Miscanthus sinensis*

After GH10 hydrolysis, three oligosaccharides co-eluted with  $X_1$ ,  $X_2$  and  $X_3$  of the xylooligosaccharide standards in DASH. We identified nine additional peaks from oligosaccharides of unknown structure which were named  $N_1$ – $N_9$  (Fig. 2). The [Me]GlcA modified hydrolysis products mainly accumulated in earlier SEC fractions independent of their molecular size (Fig. 3, fractions *Ms10\_24–46*) because of the negative charge of the Bio-Gel P2, which results in the exclusion of uronic acids [39].

The oligosaccharide  $N_1$  in the DASH trace was analysed from the unfractionated GH10 miscanthus stem hydrolysis products (oligosaccharide mix prior to SEC fractionation). The  $[M+Na]^+$  ion at  $m/z$  616.0 corresponds to a  $Pent_2$  structure modified with one MeGlcA. The MALDI-CID reveals the structure of  $N_1$  as  $U^{(4Me)2}X$  (Additional file 1: Figure S3).

The  $Y_2$  ion ( $m/z$  426.0) shows there are two Xylp residues in the backbone. The presence of the significant  $Y_1$  ion ( $m/z$  294.1) indicates that the reducing-end Xylp is unsubstituted. The  $^{0,2}X_1$  ion ( $m/z$  523.9) indicates that the non-reducing-end Xylp is modified at the O-2 with a MeGlcA, while the presence of the  $V_3$  product ion ( $m/z$  539.9) indicates that the GlcA is modified with a methyl group at the O-4. Consistent with this,  $N_1$  oligosaccharide was sensitive to GH115 glucuronidase digestion, although resistant to GH67 hydrolysis (Table 2 and Additional file 1: Figure S2A) due to it not being an ideal substrate for the GH67 enzyme [37].

The oligosaccharide  $N_2$  was in low abundance in the DASH trace and MALDI-CID showed it is the unmethylated counterpart of the  $N_3$  oligosaccharide (data not shown).

The oligosaccharide  $N_3$  in the DASH trace was analysed from fraction *Ms10\_40*. The  $[M+Na]^+$  ion at  $m/z$  748.1 corresponds to a  $Pent_3$  structure modified

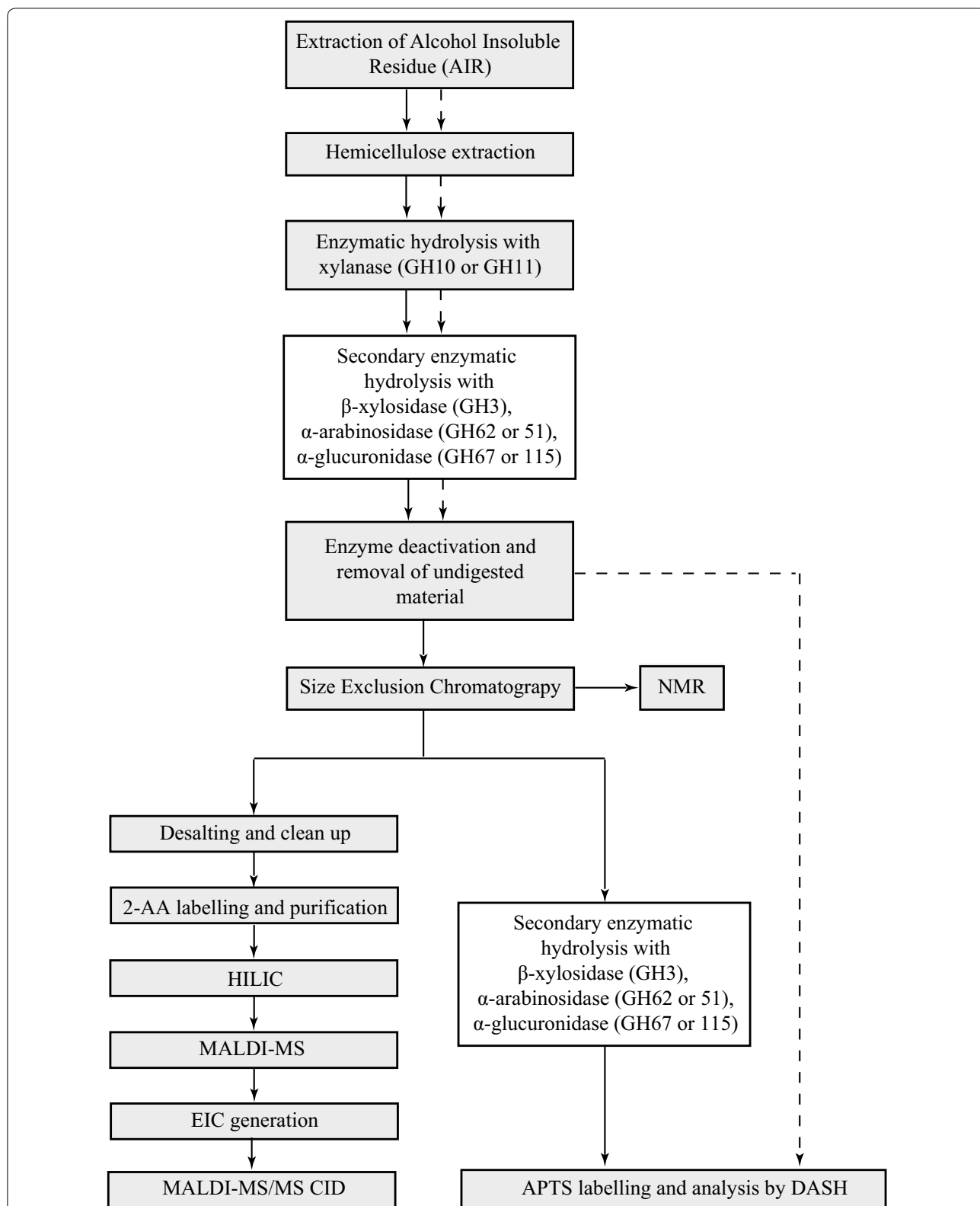


**Fig. 1** Overview of the technical procedure used to characterise GAX structures. Creation of the GAX oligosaccharide library from *Miscanthus sinensis* including extensive structural analysis (solid lines), generation of standard DASH profiles prior to SEC (dashed lines). White filled boxes indicate optional steps

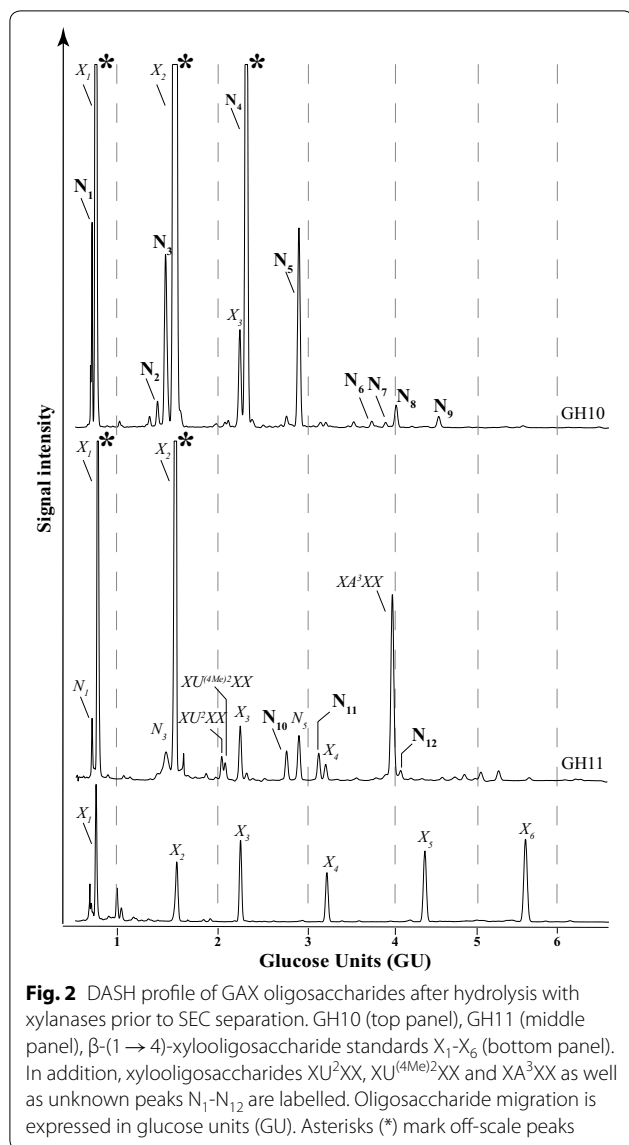


**Fig. 2** DASH profile of GAX oligosaccharides after hydrolysis with xylanases prior to SEC separation. GH10 (top panel), GH11 (middle panel),  $\beta$ -(1  $\rightarrow$  4)-xylooligosaccharide standards  $X_1$ – $X_6$  (bottom panel). In addition, xylooligosaccharides  $XU^2XX$ ,  $XU^{(4Me)2}XX$  and  $XA^3XX$  as well as unknown peaks  $N_1$ – $N_{12}$  are labelled. Oligosaccharide migration is expressed in glucose units (GU). Asterisks (\*) mark off-scale peaks

with one MeGlcA. The MALDI-CID reveals the structure of  $N_3$  as  $U^{(4Me)2}XX$  (Additional file 1: Figure S4): The series of Y and cross-ring  $^{1,5}X$  ions gives crucial sequence information showing the positioning of the [Me]GlcA on the xylan backbone. The cross-ring  $^{0,2}X_2$  ion ( $m/z$  655.9) indicates that the non-reducing-end  $Xylp$  is modified at the O-2 with a methylated uronic acid. The non-reducing end  $E_2$  ( $m/z$  461.0) product ion confirms this linkage assignment and the presence of  $V_4$  ( $m/z$  671.9) product ion indicates that the GlcA is modified with a methyl group at the O-4. The  $N_3$  oligosaccharide was susceptible to digestion with GH67 and GH115 glucuronidase (Table 2 and Additional file 1: Figure S2A), with the GH67-sensitivity confirming that the GlcA substitution is at the non-reducing end.

The oligosaccharide  $N_4$  in the DASH trace was analysed from fraction  $Ms10_{75}$ . The  $[M + Na]^+$  ion at  $m/z$  558.1 corresponds to a  $Pent_3$  structure, but it does not co-migrate with  $Xyl_3$  in DASH, suggesting it is a substituted  $Xyl_2$ . The MALDI-CID reveals the structure of  $N_4$  as  $A^3X$  (Additional file 1: Figure S5): A major  $Y_1$  ion ( $m/z$  294.1) is indicative of an unsubstituted reducing-end  $Xylp$ . The presence of the  $^{0,2}X_1$  ion ( $m/z$  336.1) and the  $E_2$  product ion ( $m/z$  271.1) indicates that the second  $Xylp$  from the reducing-end is unsubstituted at the O-2. The presence of the  $G_3$  ion ( $m/z$  510.7) indicates the pentose substitution is Araf. Consistent with this,  $N_4$  oligosaccharide was sensitive to GH62 and GH51 arabinosidase digestions (Table 2).

The oligosaccharide  $N_5$  in the DASH trace was analysed from fraction  $Ms10_{65}$ . The  $[M + Na]^+$  ion at  $m/z$  690.1 corresponds to a  $Pent_4$  structure, but it does not co-migrate with  $Xyl_4$  in DASH suggesting it is a substituted  $Xyl_3$ . The MALDI-CID reveals the structure of  $N_5$  as  $XA^3X$  (Additional file 1: Figure S6).

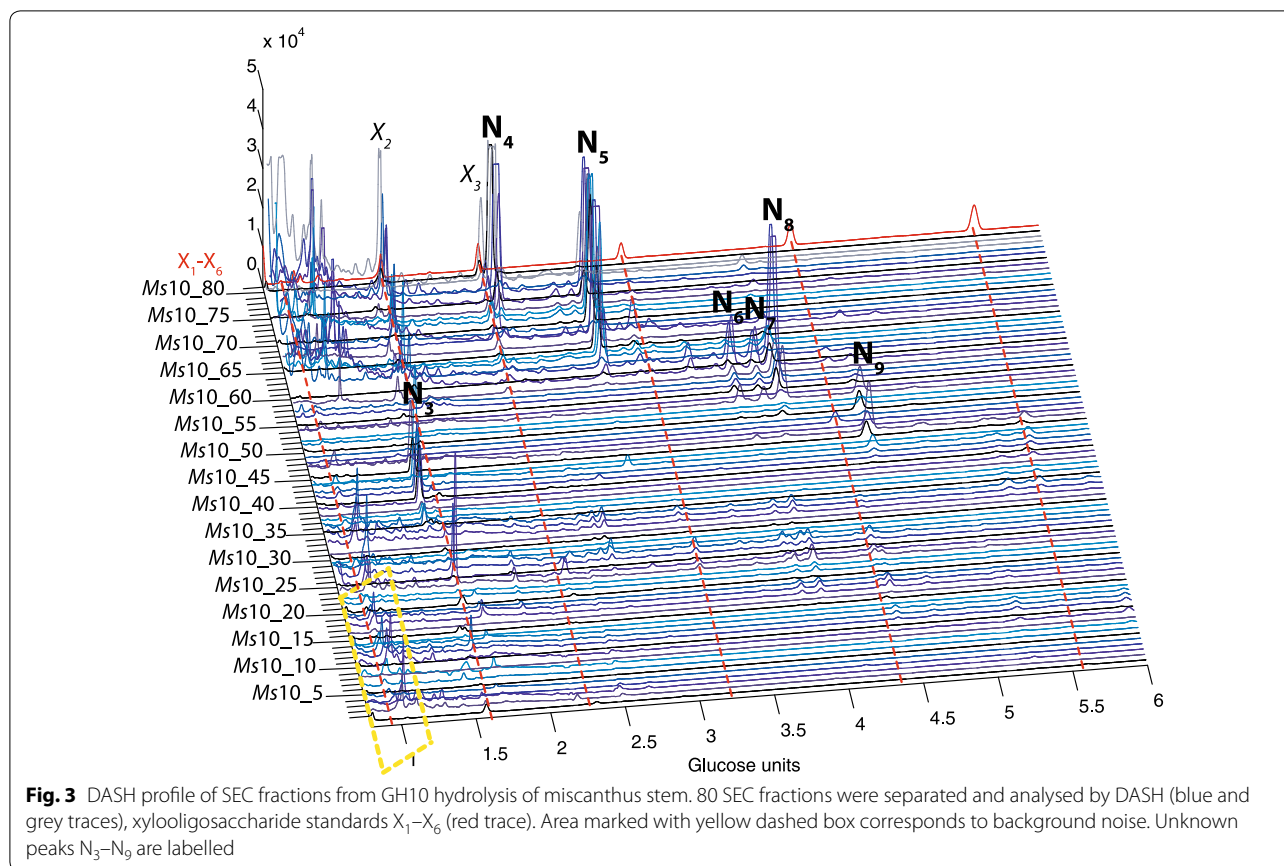
The  $^{1,5}X$  ion shows that the 2-AA-derivatised reducing-end  $Xylp$  is not modified. The cross-ring  $^{0,2}X_1$  ion ( $m/z$  336.1) indicates that the O-2 in the middle  $Xylp$  is also not substituted. This is supported by the presence of the  $E_2$  ( $m/z$  403.1) product ion, while the presence of the  $W_2$  sugar lactone ion ( $m/z$  424.1) [29] indicates that the middle  $Xylp$  is substituted at O-3 with a pentose residue. The presence of the  $G_{3\alpha}$  ion ( $m/z$  642.0) indicates the substitution is Araf. Consistent with this, the  $N_5$  oligosaccharide was sensitive to GH62 and GH51 arabinosidase digestions (Table 2).

The oligosaccharides  $N_6$ – $N_8$  in the DASH trace were analysed from fraction  $Ms10_{55}$  (Fig. 4a, the structure  $N_9$  was more abundant in fraction  $Ms10_{45}$  and corresponds to a  $Pent_6$  oligosaccharide).  $N_6$ – $N_8$  oligosaccharides had the same  $m/z$  822.0  $[M + Na]^+$  corresponding to  $Pent_5$  structural isomers (Fig. 4b). The extracted ion chromatogram (EIC) from off-line HILIC-MALDI-CID mass spectrometry of 2-AA labelled SEC fractions showed that  $Ms10_{55}$ , contained three structural isomers of  $Pent_5$  observed as  $[M + Na]^+$  at  $m/z$  822.0 ( $Z_1$ – $Z_3$ , Fig. 4c).

Arabinofuranosidase digestion of the oligosaccharides followed by DASH and HILIC-MALDI showed that the oligosaccharides  $Z_1$ ,  $Z_2$  and  $Z_3$  correspond to  $N_6$ ,  $N_7$  and  $N_8$  (Table 2).

The MS/MS spectra for  $N_6$ ,  $N_7$  and  $N_8$  oligosaccharides are shown in Fig. 5.

The presence of the G ions ( $m/z$  773.9) in the  $N_6$ ,  $N_7$  and  $N_8$  spectra indicates Araf substitution. The presence of the  $^{1,5}X_1$  cross-ring ion showed that the 2-AA labelled reducing-end  $Xylp$  is not substituted in any of the three structural isomers. The significant  $Y_2$ ,  $^{1,5}X_2$  and  $^{0,2}X_2$  ions ( $m/z$  426.1, 454.0 and 468.1, respectively) in the spectra



of  $N_7$  and  $N_8$  indicate that the second  $Xylp$  residue from the reducing end is also not substituted. In contrast, the absence of these ions from the  $N_6$  spectrum and the concomitant presence of the  $W_2$  ( $m/z$  424.1) sugar lactone ion indicate that in this isomer the second  $Xylp$  residue from the reducing-end is substituted at  $O$ -3. The presence of the  $G_3$  product ion at  $m/z$  656.0 in the spectrum of  $N_6$  indicates that the third  $Xylp$  residue from the reducing end is also substituted at the  $O$ -3 with  $Araf$ . This is confirmed by the presence of the  $E_2$  ( $m/z$  271.1) product ion which indicates that the third  $Xylp$  from the reducing end is not substituted at  $O$ -2. Hence the  $N_6$  structure was identified as  $A^3A^3X$ . Consistent with this, the  $N_6$  oligosaccharide was sensitive to GH51 arabinosidase digestion. Possibly, due to steric hindrance of  $Araf$  substitutions on two consecutive  $Xylp$  residues,  $N_6$  was resistant to GH62 hydrolysis (Table 2).

The presence of the series of  $B$ ,  $Y$  and  $^{15}X$  ions differing by 132 Da in the MALDI-CID spectra of the  $N_7$  and  $N_8$  structural isomers, indicates the linear sequence of pentoses. Based on the MALDI-CID spectra alone the precise structure of  $N_7$  and  $N_8$  oligosaccharides could not be identified. However,  $N_7$  was found to be sensitive to both GH62 and GH51 arabinofuranosidases, while  $N_8$  was

resistant to both enzymes. Taking the MALDI-CID data and the information from enzyme sensitivity together,  $N_7$  was identified as  $A^3XXX$ .  $N_8$  was further analysed by Nuclear Magnetic Resonance (NMR) to gain further insight into the detailed structure of this oligosaccharide (Fig. 5d and Additional file 2: Table S1).

Chemical-shift assignments were obtained using 2D  $^1H$ - $^1H$  TOCSY (Total Correlated Spectroscopy) and ROESY (Rotating-frame Overhauser Effect Spectroscopy) alongside 2D  $^{13}C$  HSQC (Heteronuclear Single Quantum Correlation) and HSQC-TOCSY experiments. The non-reducing-end  $Xylp$  residue was readily identified and the chemical shifts of the H-1 and C-1 were consistent with a  $\beta$  configuration. The  $Xylp$  (1  $\rightarrow$  2) linkage to  $\alpha$ - $Araf$  was apparent from the intense NOE from  $Xylp$  H-1 to  $Araf$  H-2 taken together with the downfield shift of  $Araf$  C-2 characteristic of a glycosidic bond. The  $Araf$ -(1  $\rightarrow$  3)- $Xylp$  and  $Xylp$ -(1  $\rightarrow$  4)- $Xylp$  links were also confirmed by a combination of NOEs and the downfield  $^{13}C$  shifts of the linked carbon. H3 and H4 assignments of  $\beta$ - $Xylp$  were apparent from relative TOCSY and NOESY intensities of the cross-peak connecting to H1 (both were stronger for H3). The reducing-end  $Xylp$  could not be identified due to peak broadening and overlap (the

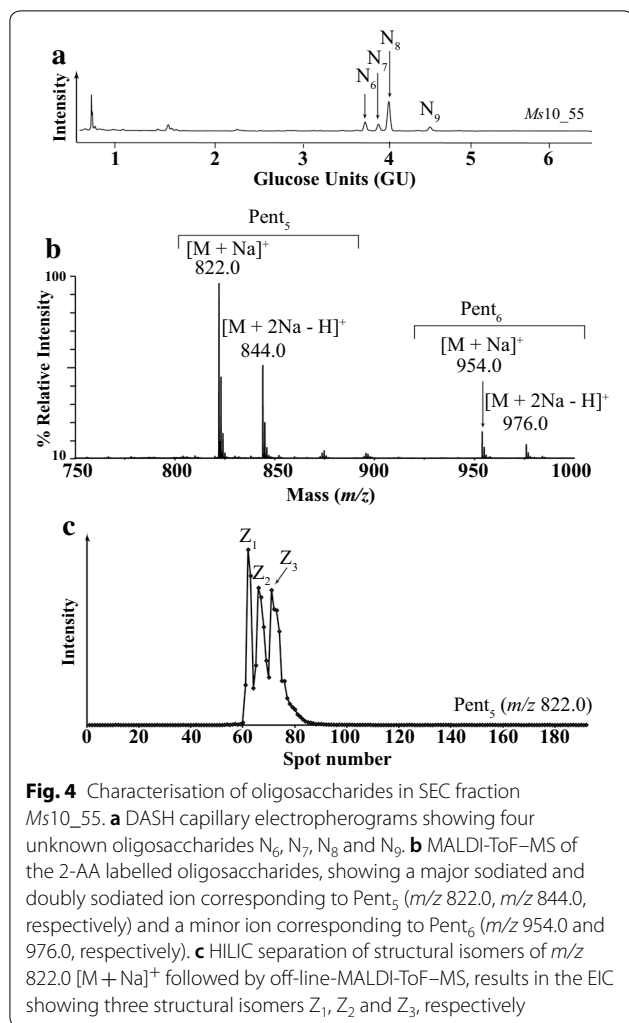
**Table 1 Structures of GAX oligosaccharides and their migration positions by DASH expressed in glucose units (GU)**

Nomenclature	Structure	Unknown structure	MALDI-CID or NMR figure	Glucose units
U <sup>(4Me)<sup>2</sup></sup> X	4-O-Me- $\alpha$ -Glc pA-(1 $\rightarrow$ 2)- $\beta$ -Xyl p-(1 $\rightarrow$ 4)-Xyl p	N <sub>1</sub>	S3	0.72
X	Xyl p			0.80
U <sup>2</sup> XX	$\alpha$ -Glc pA-(1 $\rightarrow$ 2)- $\beta$ -Xyl p-(1 $\rightarrow$ 4)- $\beta$ -Xyl p-(1 $\rightarrow$ 4)-Xyl p	N <sub>2</sub>		1.40
U <sup>(4Me)<sup>2</sup></sup> XX	4-O-Me- $\alpha$ -Glc pA-(1 $\rightarrow$ 2)- $\beta$ -Xyl p-(1 $\rightarrow$ 4)- $\beta$ -Xyl p-(1 $\rightarrow$ 4)-Xyl p	N <sub>3</sub>	S4	1.48
X <sub>2</sub>	$\beta$ -Xyl p-(1 $\rightarrow$ 4)-Xyl p			1.57
XU <sup>2</sup> XX	$\beta$ -Xyl p-(1 $\rightarrow$ 4)-[ $\alpha$ -Glc pA-(1 $\rightarrow$ 2)]- $\beta$ -Xyl p-(1 $\rightarrow$ 4)- $\beta$ -Xyl p-(1 $\rightarrow$ 4)-Xyl p			2.03
XU <sup>(4Me)<sup>2</sup></sup> XX	$\beta$ -Xyl p-(1 $\rightarrow$ 4)-[4-O-Me- $\alpha$ -Glc pA-(1 $\rightarrow$ 2)]- $\beta$ -Xyl p-(1 $\rightarrow$ 4)- $\beta$ -Xyl p-(1 $\rightarrow$ 4)-Xyl p			2.07
X <sub>3</sub>	$\beta$ -Xyl p-(1 $\rightarrow$ 4)- $\beta$ -Xyl p-(1 $\rightarrow$ 4)-Xyl p			2.24
A <sup>3</sup> X	$\alpha$ -Araf-(1 $\rightarrow$ 3)- $\beta$ -Xyl p-(1 $\rightarrow$ 4)-Xyl p	N <sub>4</sub>	S5	2.31
A <sup>3</sup> U <sup>(4Me)<sup>2</sup></sup> XX	$\alpha$ -Araf-(1 $\rightarrow$ 3)- $\beta$ -Xyl p-(1 $\rightarrow$ 4)-[4-O-Me- $\alpha$ -Glc pA-(1 $\rightarrow$ 2)]- $\beta$ -Xyl p-(1 $\rightarrow$ 4)- $\beta$ -Xyl p-(1 $\rightarrow$ 4)-Xyl p	N <sub>10</sub>	S8	2.74
XA <sup>3</sup> X	$\beta$ -Xyl p-(1 $\rightarrow$ 4)-[ $\alpha$ -Araf-(1 $\rightarrow$ 3)]- $\beta$ -Xyl p-(1 $\rightarrow$ 4)-Xyl p	N <sub>5</sub>	S6	2.87
B <sup>2,3</sup> U <sup>(4Me)<sup>2</sup></sup> XX or D <sup>2,3</sup> U <sup>(4Me)<sup>2</sup></sup> XX	Araf-(1 $\rightarrow$ 2)- $\alpha$ -Araf-(1 $\rightarrow$ 3)- $\beta$ -Xyl p-(1 $\rightarrow$ 4)-[ $\alpha$ -Glc pA-(1 $\rightarrow$ 2)]- $\beta$ -Xyl p-(1 $\rightarrow$ 4)- $\beta$ -Xyl p-(1 $\rightarrow$ 4)-Xyl p	N <sub>11</sub>	S9	3.09
D <sup>2,3</sup> X	$\beta$ -Xyl p-(1 $\rightarrow$ 2)- $\alpha$ -Araf-(1 $\rightarrow$ 3)- $\beta$ -Xyl p-(1 $\rightarrow$ 4)-Xyl p	M <sub>1</sub>	S12	3.12
X <sub>4</sub>	$\beta$ -Xyl p-(1 $\rightarrow$ 4)- $\beta$ -Xyl p-(1 $\rightarrow$ 4)- $\beta$ -Xyl p-(1 $\rightarrow$ 4)-Xyl p			3.17
A <sup>3</sup> A <sup>3</sup> X	$\alpha$ -Araf-(1 $\rightarrow$ 3)- $\beta$ -Xyl p-(1 $\rightarrow$ 4)-[ $\alpha$ -Araf-(1 $\rightarrow$ 3)]- $\beta$ -Xyl p-(1 $\rightarrow$ 4)-Xyl p	N <sub>6</sub> (Z <sub>1</sub> )	5A	3.70
A <sup>3</sup> XXX	$\alpha$ -Araf-(1 $\rightarrow$ 3)- $\beta$ -Xyl p-(1 $\rightarrow$ 4)- $\beta$ -Xyl p-(1 $\rightarrow$ 4)- $\beta$ -Xyl p-(1 $\rightarrow$ 4)-Xyl p	N <sub>7</sub> (Z <sub>2</sub> )	5B	3.85
XA <sup>3</sup> XX	$\beta$ -Xyl p-(1 $\rightarrow$ 4)-[ $\alpha$ -Araf-(1 $\rightarrow$ 3)]- $\beta$ -Xyl p-(1 $\rightarrow$ 4)- $\beta$ -Xyl p-(1 $\rightarrow$ 4)-Xyl p			3.92
D <sup>2,3</sup> XX	$\beta$ -Xyl p-(1 $\rightarrow$ 2)- $\alpha$ -Araf-(1 $\rightarrow$ 3)- $\beta$ -Xyl p-(1 $\rightarrow$ 4)- $\beta$ -Xyl p-(1 $\rightarrow$ 4)-Xyl p	N <sub>8</sub> (Z <sub>3</sub> )	5C 5D	3.97
XA <sup>3</sup> XU <sup>(4Me)<sup>2</sup></sup> XX	$\beta$ -Xyl p-(1 $\rightarrow$ 4)-[ $\alpha$ -Araf-(1 $\rightarrow$ 3)]- $\beta$ -Xyl p-(1 $\rightarrow$ 4)- $\beta$ -Xyl p-(1 $\rightarrow$ 4)-[4-O-Me- $\alpha$ -Glc pA-(1 $\rightarrow$ 2)]- $\beta$ -Xyl p-(1 $\rightarrow$ 4)- $\beta$ -Xyl p-(1 $\rightarrow$ 4)-Xyl p	N <sub>12</sub>	S10	4.01
X <sub>5</sub>	$\beta$ -Xyl p-(1 $\rightarrow$ 4)- $\beta$ -Xyl p-(1 $\rightarrow$ 4)- $\beta$ -Xyl p-(1 $\rightarrow$ 4)- $\beta$ -Xyl p-(1 $\rightarrow$ 4)-Xyl p			4.32
XA <sup>3</sup> A <sup>3</sup> X	$\beta$ -Xyl p-(1 $\rightarrow$ 4)-[ $\alpha$ -Araf-(1 $\rightarrow$ 3)]- $\beta$ -Xyl p-(1 $\rightarrow$ 4)-[ $\alpha$ -Araf-(1 $\rightarrow$ 3)]- $\beta$ -Xyl p-(1 $\rightarrow$ 4)-Xyl p	N <sub>9</sub>	S7	4.47
XD <sup>2,3</sup> XX	$\beta$ -Xyl p-(1 $\rightarrow$ 4)-[ $\beta$ -Xyl p-(1 $\rightarrow$ 2)- $\alpha$ -Araf-(1 $\rightarrow$ 3)]- $\beta$ -Xyl p-(1 $\rightarrow$ 4)- $\beta$ -Xyl p-(1 $\rightarrow$ 4)-Xyl p	M <sub>2</sub>	S11	4.83
X <sub>6</sub>	$\beta$ -Xyl p-(1 $\rightarrow$ 4)- $\beta$ -Xyl p-(1 $\rightarrow$ 4)- $\beta$ -Xyl p-(1 $\rightarrow$ 4)- $\beta$ -Xyl p-(1 $\rightarrow$ 4)- $\beta$ -Xyl p-(1 $\rightarrow$ 4)-Xyl p			5.54

**Table 2 Enzymatic analysis of GAX oligosaccharides**

Oligosaccharide	Unknown structure	GH10 product	GH11 product	Enzyme sensitivity				
				CgGH3 xylosidase	PcGH51 $\alpha$ -arabinosidase	PaGH62 $\alpha$ -arabinosidase	CjGH67 $\alpha$ -glucuronidase	BoGH115 $\alpha$ -glucuronidase
U <sup>(4Me)<sup>2</sup></sup> X	N <sub>1</sub>	●●	●	–	–	–	–	+
U <sup>2</sup> XX	N <sub>2</sub>	●		–	–	–	+	+
U <sup>(4Me)<sup>2</sup></sup> XX	N <sub>3</sub>	●●	●	–	–	–	+	+
A <sup>3</sup> X	N <sub>4</sub>	●●		–	+	+	NT	–
XU <sup>2</sup> XX	–		●	–	–	–	+	+
XU <sup>(4Me)<sup>2</sup></sup> XX	–		●	–	–	–	+	+
XA <sup>3</sup> X	N <sub>5</sub>	●●	●●	NT	+	+	NT	–
A <sup>3</sup> A <sup>3</sup> X	N <sub>6</sub> (Z <sub>1</sub> )	●		NT	+	–	NT	–
A <sup>3</sup> XXX	N <sub>7</sub> (Z <sub>2</sub> )	●		NT	+	+	NT	NT
XA <sup>3</sup> XX	–		●●	–	NT	+	NT	–
D <sup>2,3</sup> XX	N <sub>8</sub> (Z <sub>3</sub> )	●		+	–	–	NT	–
XA <sup>3</sup> A <sup>3</sup> X	N <sub>9</sub>	●		–	+	–	NT	NT
A <sup>3</sup> U <sup>(4Me)<sup>2</sup></sup> XX	N <sub>10</sub>		●	NT	+	–	NT	–
B <sup>2,3</sup> U <sup>(4Me)<sup>2</sup></sup> XX or D <sup>2,3</sup> U <sup>(4Me)<sup>2</sup></sup> XX	N <sub>11</sub>		●	–	–	NT	NT	–
XA <sup>3</sup> XU <sup>(4Me)<sup>2</sup></sup> XX	N <sub>12</sub>		●	NT	+	+	NT	+
D <sup>2,3</sup> X	M <sub>1</sub>	●		+	–	–	NT	–
XD <sup>2,3</sup> XX	M <sub>2</sub>		●	+	–	–	NT	–

The dots indicate, which xylanase produces the oligosaccharide; one dot (●) indicates minor products while two dots (●●) indicate major products. Oligosaccharides sensitive to GH enzymes are marked with a plus (+), those resistant with a minus (–); NT not tested. Oligosaccharides XU<sup>2</sup>XX, X<sup>(4Me)<sup>2</sup></sup>XX and XA<sup>3</sup>XX have been previously structurally characterised [27–29]



peaks for the reducing-end-adjacent *Xylp* are also significantly broadened). Our chemical-shift assignments are in accordance with previous  $^1H$  and  $^{13}C$  NMR analysis of a feruloylated  $D^{2,3}X$  oligosaccharide from shoots of wiregrass (*Cynodon dactylon*) [40], except the nuclei involved in the feruloyl linkage. Therefore, structure  $N_8$  was identified as  $D^{2,3}XX$ . In addition, this structure was found to be sensitive to a GH3  $\beta$ -xylosidase (*CgGH3*) that cleaves terminal *Xylp* residues from  $\beta$ -*Xylp*-(1  $\rightarrow$  2)-*Araf*-(1  $\rightarrow$  3)-*Xylp* structures, confirming the assignment (Table 2).

The oligosaccharide  $N_9$  in the DASH trace was analysed from fraction *Ms10\_45*. The  $[M + Na]^+$  ion at  $m/z$  954.3 corresponds to a  $Pent_6$  structure. The MALDI-CID reveals the structure of  $N_9$  as  $XA^3A^3X$  (Additional file 1: Figure S7).

The  $^{1,5}X_1$  ( $m/z$  322.1) and the  $Y_1$  ( $m/z$  294.2) ions show that the reducing-end *Xylp* residue is unsubstituted. The reducing-end  $G_2$  ( $m/z$  392.2) and  $G_3$  ( $m/z$  656.1) product

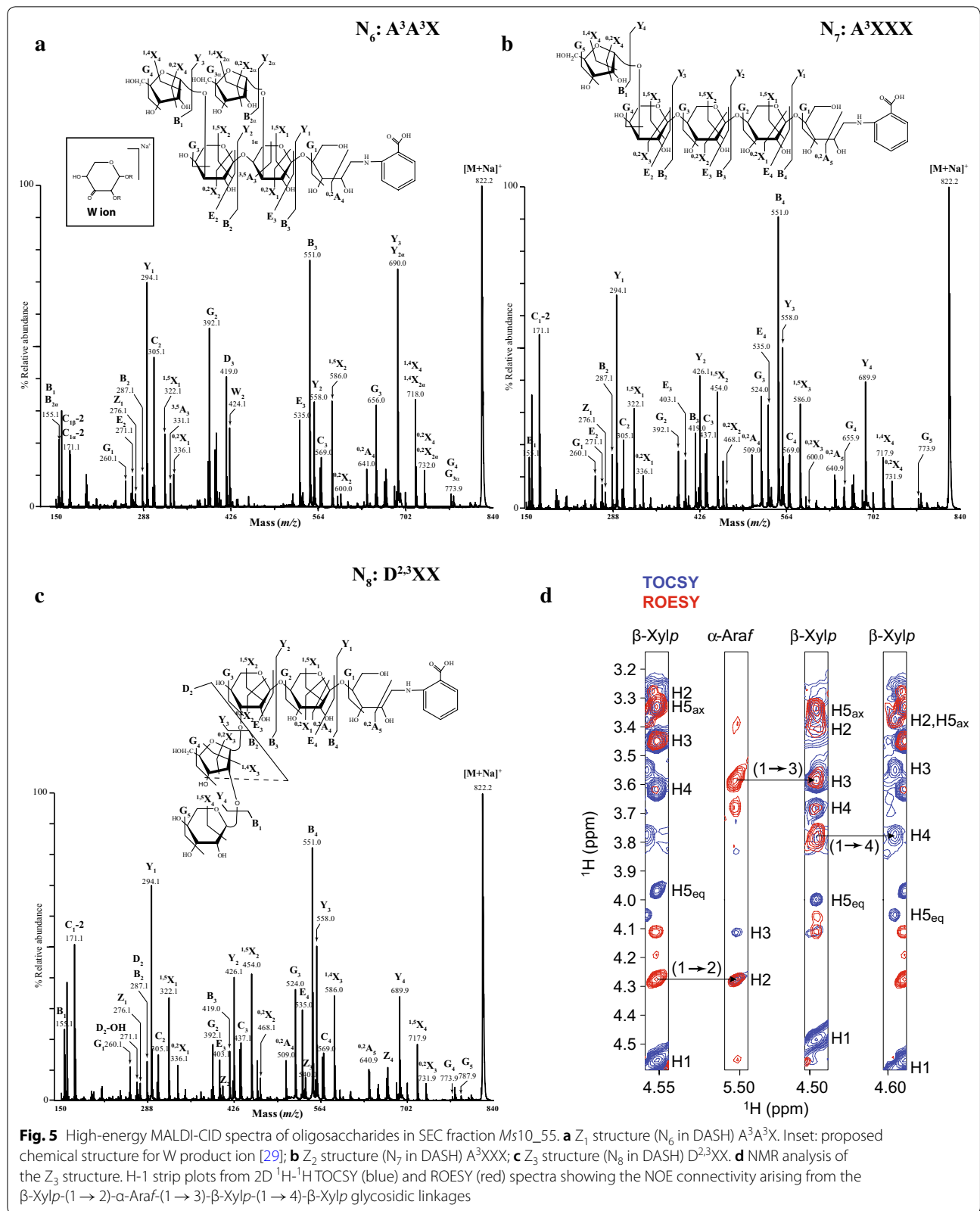
ions show that the second and third *Xylp* residues from the reducing end are substituted at *O*-3. The presence of the  $G3_\alpha/G4_\beta$  ion ( $m/z$  906.4, loss of 48 Da) indicate the presence of at least one terminal *Araf*. GH51 arabinosidase hydrolysis resulted in an oligosaccharide co-migrating with xylotetraose ( $X_4$ ; data not shown), confirming that both pentose substitutions are *Araf* residues. Similar to  $N_6$  oligosaccharide,  $N_9$  was resistant to GH62 arabinosidase hydrolysis (Table 2 and Additional file 1: Figure S2C).

#### Structural characterisation of the oligosaccharides $N_{10}$ , $N_{11}$ and $N_{12}$ from the xylanase GH11 digest of *Miscanthus sinensis*

After GH11 hydrolysis, four oligosaccharides co-eluted with  $X_1$ ,  $X_2$ ,  $X_3$  and  $X_4$  of the xylooligosaccharide standards; three oligosaccharides were structurally characterised with high-energy MALDI-CID and were identical to the previously characterised xylooligosaccharides:  $XU^2XX$  and  $XU^{(4Me)2}XX$  and  $XA^3XX$ . Furthermore, three oligosaccharides,  $N_1$ ,  $N_3$  and  $N_5$ , were identified based on their GU unit assigned from the GH10 library. However, we also identified three additional peaks from oligosaccharides of unknown structure which were named  $N_{10}$ – $N_{12}$ . For the detailed structural characterisation of these oligosaccharides, the GH11 oligosaccharide mixture was loaded on a SEC column (Additional file 1: Figure S1 fractions *Ms11\_01* to *Ms11\_80*) and unknown structures were consequently analysed by high-energy MALDI-CID.

The oligosaccharide  $N_{10}$  in the DASH trace was analysed from fraction *Ms11\_05*. The  $[M + Na]^+$  ion at  $m/z$  1012.8 corresponds to a  $Pent_5$  structure modified with one MeGlcA. The MALDI-CID reveals the structure of  $N_{10}$  as  $A^3U^{(4Me)2}XX$  (Additional file 1: Figure S8): The presence of the  $Y_1$  ( $m/z$  294.3) and  $Y_2$  ( $m/z$  426.3) ions indicate that the reducing end and the adjacent *Xylp* are unsubstituted. The  $E_3$  ion ( $m/z$  403.4) and  $H_3$  ( $m/z$  435.3) sugar lactone indicate that the third *Xylp* from the reducing end is modified at *O*-2 with a methylated glucuronic acid, while the  $V_{3\alpha}$  product ion ( $m/z$  936.3) indicates that the GlcA is modified with a methyl group at *O*-4. The series of  $Y_3$  ( $m/z$  748.3) and  $Y_4$  ( $m/z$  880.2) indicate that two pentosyl residues are present at the non-reducing end while the absence of the non-reducing end  $^{3,5}A_2$  ion ( $m/z$  199.0) indicates that the non-reducing end *Xylp* is substituted by a pentose. Finally the presence of the  $G_4$  reducing-end ion ( $m/z$  846.3) is indicative of a substitution at *O*-3 of the reducing-end *Xylp* residue. The  $N_{10}$  oligosaccharide was found sensitive to GH51 hydrolysis indicating that the pentosyl modification on the fourth *Xylp* residue from the reducing end is an *Araf* residue (Table 2).





The oligosaccharide  $N_{11}$  in the DASH trace was analysed from fraction *Ms11\_70*. The  $[M+Na]^+$  ion at  $m/z$  1144.8 corresponds to a  $Pent_6$  structure modified with one MeGlcA. The MALDI-CID combined with enzymatic hydrolysis was not conclusive but indicates two putative structures of  $N_{11}$  as  $B^{2,3}U^{(4Me)2}XX$  or  $D^{2,3}U^{(4Me)2}XX$  (Additional file 1: Figure S9).

The presence of the  $Y_1$  ( $m/z$  294.3) and  $Y_2$  ( $m/z$  426.3) ions indicated that the reducing end and the adjacent  $Xylp$  are unsubstituted. The  $E_4$  ion ( $m/z$  535.4) and  $H_4$  ( $m/z$  567.3) sugar lactone indicate that the third  $Xylp$  from the reducing end is modified at *O*-2 with a MeGlcA. This assignment is also confirmed by the presence of the  $G_3$  reducing-end ion ( $m/z$  714.3). The  $V_{3\alpha}$  product ion ( $m/z$  1068.3) indicated that the GlcA was modified with a methyl group at the *O*-4 position. The presence of a series of  $Y$  ions,  $Y_4$  ( $m/z$  880.2) and  $Y_5$  ( $m/z$  1012.2), indicates that the reducing-end sugar sequence of this oligosaccharide is a linear pentose chain. However, the presence of  $G_4$  ion ( $m/z$  846.3) indicated that the fourth  $Xylp$  residue from the reducing end is modified at *O*-3. Furthermore the reducing-end  $^{0,2}X_4$  ion ( $m/z$  1054.3) is indicative of a modification at *O*-2 of the fifth pentosyl group from the reducing end and therefore pointing to a structure similar to the  $D^{2,3}XX$  (Fig. 5c).  $N_{11}$  oligosaccharide was resistant to *CgGH3* xylosidase which would be in accordance with the  $B^{2,3}U^{(4Me)2}XX$  assignment or could be explained by steric hindrance by MeGlcA modification on the adjacent  $Xylp$  residue in the case of  $D^{2,3}U^{(4Me)2}XX$  assignment (Table 2).

The oligosaccharide  $N_{12}$  in the DASH trace was analysed from fraction *Ms11\_05*. The  $[M+Na]^+$  ion at  $m/z$  1276.9 corresponds to a  $Pent_7$  structure modified with one MeGlcA. The MALDI-CID combined with enzymatic hydrolysis reveals the structure of  $N_{12}$  as  $XA^3XU^{(4Me)2}XX$  (Additional file 1: Figure S10).

The series of  $Y$  ions ( $Y_1, Y_2, Y_3, Y_4$  and  $Y_5$ ;  $m/z$  294.4,  $m/z$  426.4,  $m/z$  748.3,  $m/z$  880.3 and  $m/z$  1144.2, respectively) indicate that the oligosaccharide is modified on the third  $Xylp$  residue from the reducing end with  $[Me]GlcA$  and also on the fifth  $Xylp$  residue from the reducing end with a pentosyl group. The presence of  $H_3$  ( $m/z$  699.4) sugar lactone confirms that the third  $Xylp$  residue is modified by a  $[Me]GlcA$  and indicates that this modification is at *O*-2. Additionally, the presence of  $G_5$  ( $m/z$  978.3) reducing-end ions indicates that the fifth  $Xylp$  residue is modified at *O*-3. The  $V_{3\alpha}$  product ion ( $m/z$  1200.4) indicates that the GlcA was modified with a methyl group at *O*-4. This oligosaccharide was found sensitive to *GH51* and *GH62* hydrolysis, indicating that the pentosyl modification on the fifth  $Xylp$  residue from the reducing end is an *Araf* residue,

and to *GH115* hydrolysis confirming that the uronic acid modification on the third  $Xylp$  from the reducing end is a  $[Me]GlcA$  (Table 2 and Additional file 1: Figure S2A).

#### Comparative structural analysis of GAX oligosaccharides derived from different grasses and different tissues

The developed reference library was used to characterise variation of GAX in agriculturally important grasses in different aerial tissues. We analysed the xylooligosaccharide products of *GH10* and *GH11* hydrolysis from stems and leaves of brachypodium, maize, rice, sugar cane, wheat, leaves of miscanthus and stems of barley as well as sugar cane bagasse (Figs. 6 and 7).

The DASH profiles of the xylooligosaccharides of the *GH10* and the *GH11* digests of all grasses analysed look very similar and nearly all peaks can be annotated based on the GU of their oligosaccharides. The main peaks are  $X_1, X_2, A^3X$  and  $XA^3X$ , respectively. Overall, arabinosylation appears more abundant than glucuronidation and the latter seems more variable in abundance across grasses. In addition, the ratio of methylated and unmethylated GlcA seems to widely differ in grasses with rice GAX being rather unmethylated, whereas major proportion of GlcA in, e.g. miscanthus and sugar cane GAX is methylated. There is also a slight variance in abundance of the more complex oligosaccharides. Moreover, we can detect additional peaks: The most characteristic peaks,  $M_1$  and  $M_2$ , are present in the DASH profiles of leaf GAX from all grasses analysed, but very rare in GAX of stem with the exception of rice stem GAX, in which  $M_1$  and  $M_2$  are substantial.

#### Structural characterisation of the oligosaccharides $M_1$ and $M_2$ from leaf GAX

In order to identify the unknown oligosaccharides  $M_1$  and  $M_2$ , maize leaf *GH10* and rice leaf *GH11* oligosaccharide products, respectively, were separated by SEC. The suitable SEC fractions (*Zm10\_65* for structure  $M_1$  and *Os11\_60* for structure  $M_2$ ) were further analysed by MALDI-ToF/ToF Mass Spectrometry, structural isomers were separated by HILIC and structurally characterised by high-energy MALDI-CID (Additional file 1: Figure S11).

The oligosaccharide  $M_1$  in the DASH trace was analysed from fraction *Zm10\_65* (Additional file 1: Figure S11A). The unknown oligosaccharide had an  $m/z$  690.00  $[M+Na]^+$ , corresponding to a  $Pent_4$  structure (Additional file 1: Figure S11B). It did not co-migrate with  $Xyl_4$  in DASH, suggesting it is a substituted xylooligosaccharide. Off-line HILIC-MALDI-MS separated the two structural isomers with  $m/z$  690.00 ( $M_1$  and

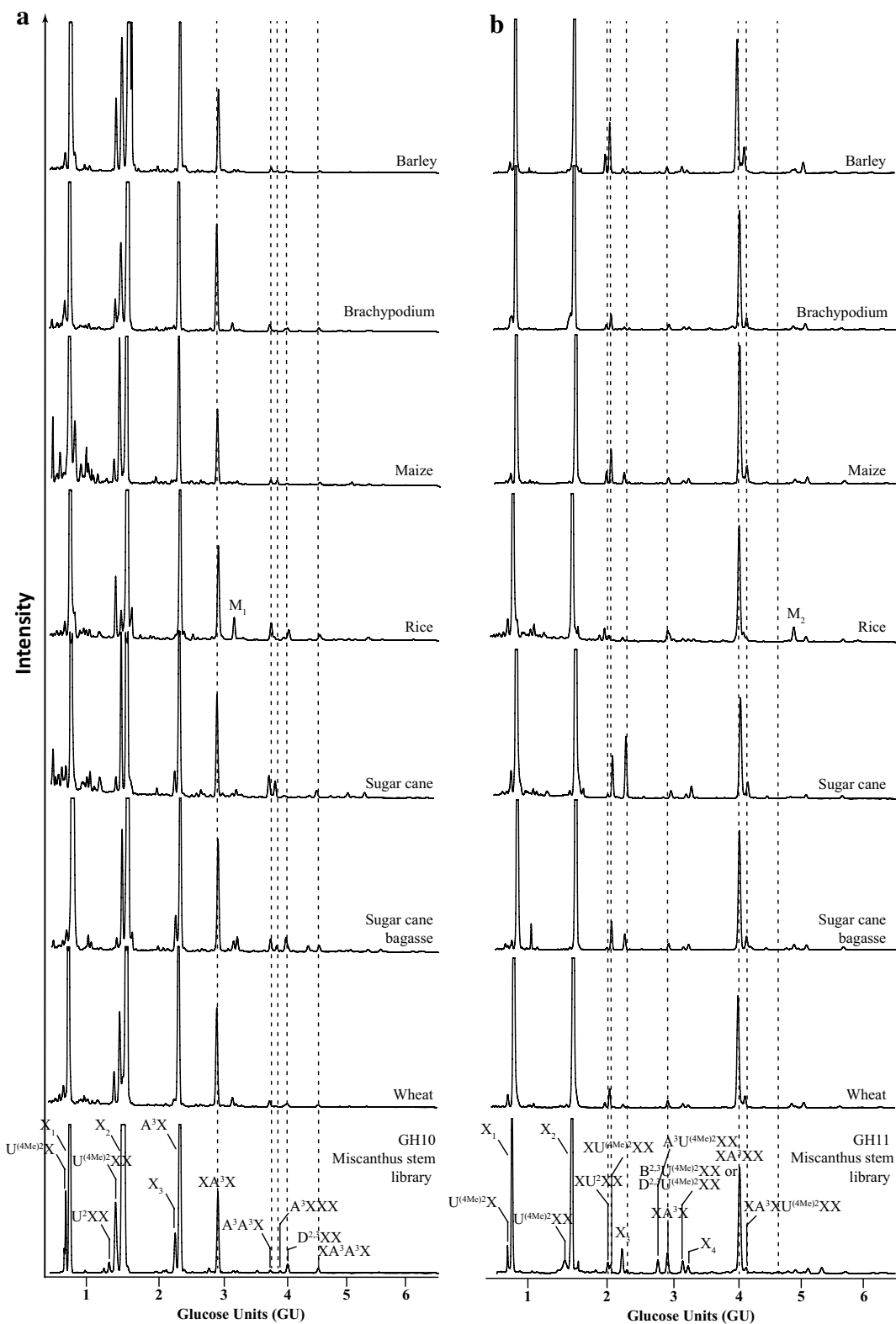
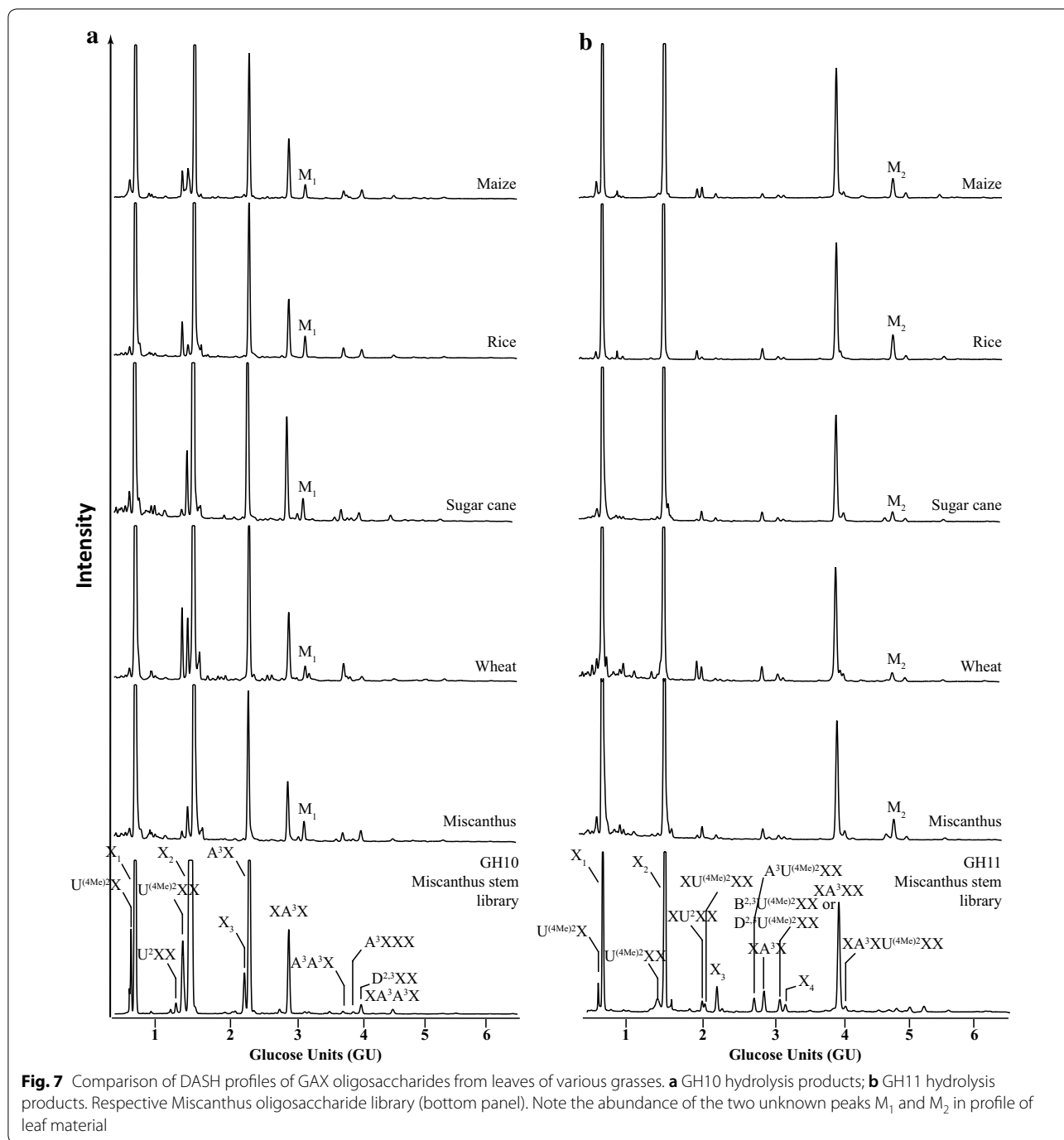


**Fig. 6** Comparison of DASH profiles of GAX oligosaccharides from stem of various grasses. **a** GH10 hydrolysis products; **b** GH11 hydrolysis products. Respective Miscanthus oligosaccharide library (bottom panel). Note the presence of two unknown peaks  $M_1$  and  $M_2$  in the rice DASH profile



$XA^3X$ , Additional file 1: Figure S11C) and the respective MALDI-CID spectra revealed the structure of  $M_1$  as  $D^{2,3}X$  (Additional file 1: Figure S12): The presence of a series of Y ions ( $Y_1$ ,  $Y_2$  and  $Y_3$ ;  $m/z$  294.3, 426.3 and 558.3, respectively) and the presence of  $^{1,4}X_2$  and  $^{1,5}X_3$  ions ( $m/z$  454.3 and 586.3, respectively) indicate that the  $M_1$  is a linear DP4 pentose chain. The presence, however, of the  $G_3$  product ion ( $m/z$  642.4, loss of 48 Da) indicates the

existence of an *Araf* residue in the structure. In addition, the presence of the  $G_4$  product ion ( $m/z$  656.5) gives evidence of a terminal *Xylp* residue on the structure. Finally, the presence of the  $^{0,2}X_2$  cross-ring ion ( $m/z$  600.3) suggests that a pentose is 2-linked on the penultimate *Xylp* residue. The assignment of  $M_1$  as  $D^{2,3}X$  was confirmed by the finding that the structure is resistant to the hydrolysis with GH62 arabinosidase, GH67 and GH115

glucuronidases, but sensitive to CgGH3  $\beta$ -xylosidase hydrolysis (Table 2 and Additional file 1: Figure S2D).

The oligosaccharide  $M_2$  in the DASH trace was analysed from fraction Os11\_60 (Additional file 1: Figure S11D). The unknown oligosaccharide had an  $m/z$  954.5  $[M+Na]^+$ , corresponding to a Pent<sub>6</sub> structure (Additional file 1: Figure S11E). It did not co-migrate with Xyl<sub>6</sub> in DASH, suggesting it is a substituted xylooligosaccharide. Off-line HILIC-MALDI-CID revealed that this was the only structural isomer present in the sample (Additional file 1: Figure S11F). The MALDI-CID revealed the structure of  $M_2$  as XD<sup>2,3</sup>XX (Additional file 1: Figure S13): The significant Y<sub>1</sub> ion ( $m/z$  294.4) and the <sup>1,5</sup>X<sub>1</sub> ion ( $m/z$  322.4) indicate that the 2-AA labelled Xylp residue is not substituted. The Y<sub>2</sub> and Y<sub>3</sub> ions ( $m/z$  426.4 and 690.4, respectively) show that the second Xylp is unsubstituted but that the third Xylp residue from the reducing end is modified with two pentose residues. The reducing-end G<sub>3</sub> ( $m/z$  524.5) product ion and the concomitant presence of the W<sub>3</sub> ( $m/z$  556.4) sugar lactone indicate that the substitution on the third Xylp from the reducing end is at O-3. This assignment is further verified by the presence of the D<sub>2</sub> ( $m/z$  271.4) product ion. The existence of the G<sub>4</sub> ( $m/z$  906.5) product ion indicates the presence of an Araf substitution. Finally, the presence of the <sup>3,5</sup>A<sub>2</sub> non-reducing end cross-ring fragment ion indicates the presence of an unsubstituted Xylp at the non-reducing end. The assignment of  $M_2$  as XD<sup>2,3</sup>XX was confirmed by the finding that the structure is resistant to the hydrolysis with GH62 arabinosidase, GH67 and GH115 glucuronidases, but sensitive to CgGH3  $\beta$ -xylosidase hydrolysis (Table 2 and Additional file 1: Figure S2D).

#### Relative quantitative differences in oligosaccharide structure and abundance in *Miscanthus sinensis* stem and leaf GAX

By DASH the relative quantity of reducing-end labelled oligosaccharides within a sample can be determined by the relative fluorescence intensity of the corresponding electropherogram peaks [27]. To analyse the difference in GAX structure in stems and leaves in greater detail, we quantified the frequency of substitution of all characterised library oligosaccharides in the GH10 and GH11 digests of three biological replicates of miscanthus using the DASHBOARD software (Fig. 8). The substitution frequency was calculated after normalisation of values by comparing the abundance of side chains to the Xylp residues in the backbone.

First of all, the overall substitution frequency of xylan with [Me]GlcA, Araf and D<sup>2,3</sup> calculated from the two different digests with GH10 and GH11, respectively, is consistent with only a minor difference for the D<sup>2,3</sup>

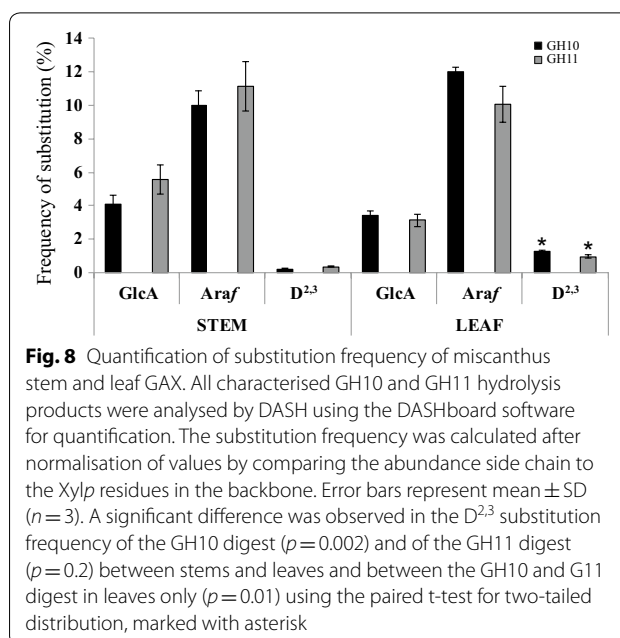


**Fig. 8** Quantification of substitution frequency of miscanthus stem and leaf GAX. All characterised GH10 and GH11 hydrolysis products were analysed by DASH using the DASHBOARD software for quantification. The substitution frequency was calculated after normalisation of values by comparing the abundance side chain to the Xylp residues in the backbone. Error bars represent mean  $\pm$  SD ( $n=3$ ). A significant difference was observed in the D<sup>2,3</sup> substitution frequency of the GH10 digest ( $p=0.002$ ) and of the GH11 digest ( $p=0.02$ ) between stems and leaves and between the GH10 and GH11 digest in leaves only ( $p=0.01$ ) using the paired t-test for two-tailed distribution, marked with asterisk

structure in leaves, showing a slightly higher frequency in the GH10 digest only (1.3% versus 1%,  $p$  value 0.01).

In both, stems and leaves of miscanthus, arabinosylation of xylan is more frequent than glucuronidation, ranging between 10 and 12% of Araf substitutions versus 3–6% of [Me]GlcA substitutions. However, there is a significant difference between tissues regarding the amount of D<sup>2,3</sup> substitution both in the GH10 ( $p$  value 0.002) and the GH11 ( $p$  value 0.02) digests. In leaves the D<sup>2,3</sup> substitution frequency of the GH10 and GH11 digest is 1.3% and 1%, respectively, whereas in stem it is down to 0.2% and 0.4%, respectively. Concomitantly, with the presence of the additional D<sup>2,3</sup> structure (D<sup>2,3</sup>X and XD<sup>2,3</sup>XX) in leaf xylan, our data show that the frequency of the D<sup>2,3</sup> structure is increased in leaves.

#### Discussion

In this study, we used a combination of SEC, DASH, HILIC and MALDI-CID to elucidate the detailed structure of grass GAX oligosaccharides released by GH10 and GH11 xylanases. Based on these data, we developed a DASH reference library of structurally identified oligosaccharides and expressed their migration in GU. It has been reported previously that DASH can separate oligosaccharides with minor structural differences like methylation of GlcA [27]. Here, we show that DASH can successfully resolve structural isomers as demonstrated by the separation of the three DP5 oligosaccharides ( $m/z$  822.0). Few approaches allow for wider screening of cell wall polysaccharide structures. Microarray-based glycan-profiling techniques [41, 42], for example, integrate the sequential extraction of glycans with the generation of

microarrays, which are probed with monoclonal antibodies (mAbs) or carbohydrate-binding molecules (CBMs) with specificities for cell wall components. Although Microarray-based glycan profiling is a powerful technique offering high-throughput analysis of a wider variety of cell wall polymers, it is limited by the availability of mAbs and CBMs and their epitope specificity. A non-destructive high-throughput method for the compositional analysis of plant cell wall polymers is Fourier Transformed Mid-Infrared (FT-IR) spectroscopy [43]. This approach can provide structural information about substitution nature and frequency of cereal arabinoxylan [44]. The DASH reference library generated here allows the fast and robust comparison of a large number of GAX samples (96 samples in 50 min), providing detailed structural and quantitative information on biomass structural variation. Information gathered from DASH analysis will ultimately greatly facilitate the biorefining selection process of appropriate biomass.

We analysed the GAX structure of a number of different grass species (miscanthus, barley, brachypodium, maize, rice, sugar cane and wheat). The DASH profiles of all grasses analysed and the quantification data of xylan substitution of *Miscanthus sinensis* showed that Araf side chains are more frequent than [Me]GlcA substitutions, which is consistent with sugar composition analysis of wheat straw [26, 45] and MS and NMR analysis of miscanthus, rice and brachypodium of the entire actively growing aerial portions [26]. Unlike cereal grain AX where 2-linked Araf residues are abundant [1, 46–48], we did not detect any such substitutions, which is consistent with earlier reports on the structure of grass GAX in lignified tissues [24, 49, 50]. The overall xylan structure of the different grass species and of the different tissues is remarkably conserved, which is in line with earlier studies on grass xylan structure [51]. However, differences between species and tissues are detectable. Interestingly, the xylan structure of rice stems appears more similar to the xylan structure in leaves than to other xylan stem structures, forming an exception in the grasses analysed, perhaps because of the immature developmental stage of the culms collected. Plants exploit a number of variations in the xylan structure that were not studied in this work, e.g. the pattern of substitutions along the xylan backbone, feruloylation and coumaroylation of Araf and acetylation of backbone Xylp. These could be studied by exploitation of additional carbohydrate active enzymes and generation of additional standards in the DASH mobility library.

The most characteristic tissue-specific differences were identified in the form of the two oligosaccharides  $D^{2,3}X$  and  $XD^{2,3}XX$ , which are (apart from in rice) scarce in stem xylan but abundant in leaf xylan. Quantification of the overall frequency of the  $D^{2,3}$  side chain in miscanthus

suggests that it is significantly more abundant in leaves than in stem. The  $D^{2,3}$  structure has been linked to feruloylation of xylan, and hence cross-linking and reduced digestibility [8]. Interestingly, the lignin amount and composition also differs in cell walls of miscanthus stems versus leaves [52]. Therefore xylan structural changes in different tissues might reflect specific levels and positioning of cross-linking, which can be a way of adjusting polymer structures to different functional requirements of the cell wall depending on its particular composition. A disaccharide side chain on xylan has been reported in sorghum [53] and switchgrass [54] although not detected by Bowman et al. [24] in a similar xylan analysis of switchgrass. The presence of this disaccharide side chain cannot be excluded although with our approach all disaccharide side-chain modifications positively identified were  $\beta$ -Xylp-(1→2)- $\alpha$ -Araf-(1→3) structures. The only exception was the GH11 product, putatively assigned as  $D^{2,3}U^{(4Me)2}XX$ , which was found resistant to CgGH3  $\beta$ -xylosidase. Resistance to CgGH3  $\beta$ -xylosidase could either be due to steric hindrance of the enzyme or could indicate the presence of an Araf-(1→2)- $\alpha$ -Araf-(1→3) side chain on this GH11 hydrolysis product ( $B^{2,3}U^{(4Me)2}XX$ ). However, the Araf-(1→2)-Araf-(1→3)-adjacent to a Xylp modified by a GlcA residue would be in a different substitution context to the Mazumder et al. [54] and Verbruggen et al. [48] reported oligosaccharides. If the latter is true then we could hypothesise that GH10 and GH11 xylanases hydrolyse slightly different parts of GAX. It is also, however, possible that the Araf-(1→2)- $\alpha$ -Araf-(1→3) side chain is not present in the tissues and plant species analysed here, or that it is present in amounts below the detection level.

It has been reported that the degree of methylation of GlcA on xylan varies between grass species and that in miscanthus methylation of xylan is more predominant than in, for example, rice or Brachypodium [49, 50]. This finding is consistent with our data on miscanthus xylan.

Some qualitative differences of oligosaccharides reflect enzyme specificity and distinct tolerance of the xylanases GH10 and GH11 to substitutions [28], for example,  $A^3X$  from GH10 and  $XA^3XX$  from GH11. However, some oligosaccharide such as  $A^3U^{(4Me)2}XX$ ,  $D^{2,3}U^{(4Me)2}XX$  (or  $B^{2,3}U^{(4Me)2}XX$ ) and  $XA^3XU^{(4Me)2}XX$ , although only minor products, were only detectable in GH11 digestion and might indicate that GH10 and GH11 act on different domains of grass xylan as they resemble different substitution patterns. The fact that the level of 3-linked Araf and [Me]GlcA substitutions is remarkably similar independent of the xylanase used does not necessarily support this hypothesis. Surprisingly, some of these minor digestion products of GH11 harbour substitutions at the non-reducing end of the oligosaccharide, which are not predicted

as products and might be the result of either using the enzymes in excess or that the GH11 enzyme preparation used in this study was contaminated with small amounts of either GH10 xylanase or  $\beta$ -xylosidase. Alternatively, these oligosaccharides could derive from the non-reducing end of the xylan polymer and would be produced by a single cleavage at the reducing end of the oligosaccharide.

## Conclusions

As characterised here in grass stems and leaves from several species, mainly three GAX sugar side chains, 3-linked Araf, 2-linked GlcA/MeGlcA and 3-linked Xylp-(1  $\rightarrow$  2)-Araf, are utilised to decorate the xylan molecule. Our GAX oligosaccharide reference library of DASH mobilities, developed in this study, provides a means to study structural aspects of xylan and might help to shed light on how structural changes of xylan correlate with the interaction of this polysaccharide with other cell wall components, how this influences its biological function, its mechanical properties and recalcitrance of the cell wall. Furthermore it provides a high-throughput quantitative method for the selection of suitable lignocellulosic biomass and tailoring of biorefining processes.

## Methods

### Plant material

The plant materials used in this study were fresh material from *Miscanthus sinensis* (miscanthus; Wageningen University, Netherlands, Luisa Trindade & Oene Dolstra), *Hordeum vulgare* (barley; University of Dundee, Claire Halpin), *Brachypodium distachyon* (Brachypodium; (grown at University of Cambridge greenhouse), *Zea mays* (maize; University of Cambridge, Paul Dupree), *Oryza sativa* (rice; grown at University of Cambridge greenhouse), *Saccharum officinarum* (sugar cane; EMBRAPA-Brazil, Christiane Farinas), sugar cane bagasse (University of Sao Paulo-Brazil, Marcos Buckridge) and *Triticum aestivum* (wheat; University of Nottingham, Greg Tucker).

### Extraction of alcohol-insoluble residue (AIR)

Plant stems and leaves were harvested, submerged in 96% (v/v) ethanol and boiled at 70 °C for 30 min to inactivate enzymes. Following homogenisation using a ball mixer mill (Glen Creston), the pellet was collected by centrifugation (4000  $\times$  g for 15 min) and was washed with 100% (v/v) ethanol, twice with chloroform:methanol (2:1), followed by successive washes with 65% (v/v), 80% (v/v) and 100% (v/v) ethanol. The remaining pellet of AIR was air dried. Aqueous suspensions (0.5 mg/ml; at 21 °C) of AIR were prepared using a glass homogeniser and kept for further analysis.

### Hemicellulose extraction

Hemicelluloses were extracted by treating AIR preparations (2 g for Size exclusion chromatography (SEC) fractionation; 50  $\mu$ g for small-scale digestions) with a small volume of 4 M NaOH (5 ml for SEC fractions; 20  $\mu$ l for small-scale digestions) for 1 h at room temperature before the pH was adjusted to about pH 6.0 with 1 N HCl; 50 mM ammonium acetate buffer pH 6.0 was added (200 ml for SEC fractionation; 0.5 ml for small-scale digestions). Note: Alkali treatments results in the removal of acetylation and feruloylation.

### Enzymatic hydrolysis and enzymes

Glycoside hydrolases of different Carbohydrate Active enZYme families were used in this study: GH10 endo- $\beta$ -1,4-xylanase CjGH10A from *Cellvibrio japonicus* [55]; GH11 endo- $\beta$ -1,4-xylanase NpGH11A from *Neocallimastix patriciarum* [56]; GH67  $\alpha$ -glucuronidase CjGH67 from *Cellvibrio japonicus* [37, 57] and GH115  $\alpha$ -glucuronidase BoGH115 from *Bacteroides ovatus* [38, 58]; GH62  $\alpha$ -arabinofuranosidase PaGH62 from *Penicillium aurantiogriseum* [59], a gift from Novozymes; GH51  $\alpha$ -arabinofuranosidase PcGH51 from *Pseudomonas cellulose* [36]; GH3 xylosidase CgGH3 from *Chaetomium globosum* (NS39127) and GH3  $\beta$ -1,4 xylosidase TrGH3 from *Trichoderma reesei* [60] were both gifts from Novozymes. All enzymes were added at a final concentration of 2  $\mu$ M and incubated at 21 °C under constant shaking for 24 h. Enzymatic hydrolysis progression was monitored by Polysaccharide Analysis Using Carbohydrate Gel Electrophoresis [61] and if necessary, the enzyme amount was adjusted to ensure complete hydrolysis.

### Enzyme deactivation and removal of undigested material

Enzymes were then deactivated by boiling for 30 min undigested cell wall material was removed by centrifugation. In case of SEC, centrifugation was followed by filtration (Whatman 45  $\mu$ m). Samples were then dried in a centrifugal evaporator.

### Size exclusion chromatography

Dried hydrolysed cell wall materials (corresponding to 2 g of AIR) were resuspended in 2 ml distilled water. Sample (2 ml) was applied onto the column and eluted with distilled water. SEC was performed on a gravity-driven Bio-Gel P-2 column (190  $\times$  2.5 cm, BioRad) as previously described [62]. 2 ml fractions were collected, concentrated to 100  $\mu$ l in a centrifugal evaporator and 10  $\mu$ l were analysed by DASH as described below. A total of 80 SEC fractions were collected for each grass species and xylanase hydrolysis analysed. The SEC fraction naming system includes information on the species (*Ms: Miscanthus*

*sinensis*, *Zm: Zea mays* and *Os: Oryza sativa*), the xylanase (10: GH10 and 11: GH11) and the fraction number (\_01 to \_80). The fractions with xylooligosaccharides of interest were subjected to secondary enzymatic hydrolysis or dried, desalted, reductively aminated with 2-anthranilic acid (2-AA), purified by HILIC and structurally characterised by high-energy MALDI-CID.

#### APTS labelling and analysis by DASH

The derivatisation of oligosaccharides with 8-aminopyrene-1,4,6-trisulfonate (APTS) was performed according to previously developed protocols [27]. A set of 7 fluorophore (DY-481XL-NHS ester)-labelled amino acids and peptides was used as electrophoretic mobility standards (Asp–Asp–Asp–Asp; Asp–Asp–Asp; Glu–Glu; Cysteic acid; L-2-Amino adipic acid; Glycine; Gly–Gly–Gly) to align the electropherograms. These electrophoretic mobility standards were mixed with each sample prior to DASH separation serving as internal mobility markers. DASH data generated by the DNA sequencer were processed with the DASHboard software [27]. Control experiments without the substrates were performed under the same conditions in order to identify any non-specific compounds in the enzymes or labelling reagents. An APTS-derivatised dextran ladder (0.1 M TFA hydrolysis at 100 °C for 2 h; 50 µg µl<sup>-1</sup> dextran in 200 µl TFA solution) was simultaneously separated by DASH and was used to provide the GU migration positions.

#### Desalting and clean up for HILIC separation

Xylooligosaccharides from SEC fractions were desalted using HyperSep Hypercarb cartridges (Thermo-Hypersil-Keystone, Runcorn, Cheshire, UK) as previously described [29]. Oligosaccharides were lyophilised and then derivatised with 2-aminobenzoic acid (2-AA) as described below.

#### Reductive amination and purification for HILIC separation

SEC-purified xylooligosaccharides were reductively aminated with 2-AA (Sigma) and then purified from the reductive amination reagents using a Glyko Clean S cartridge (Prozyme, San Leandro, CA) as previously described [63].

#### HILIC-MALDI-MS and MALDI-MS/MS CID analysis

Capillary HILIC was carried out using an LC-Packings Ultimate system (Dionex, CA, USA) equipped with an amide-80 column (300 µm × 25 cm; 3 µm particle size; Dionex) as previously described [63]. Briefly, the LC system was used to generate the gradient that flowed at 3 µl min<sup>-1</sup>. Solvent A was 50 mM ammonium formate adjusted to pH 4.4 with formic acid. Solvent B was 5% solvent A in acetonitrile. The labelled oligosaccharides

dissolved in 95% acetonitrile were loaded onto the column (20 µl) and eluted with increasing aqueous concentrations. The following gradient conditions were applied: 0 min, 5% solvent A, 95% solvent B; 6 min, 25% solvent A, 75% solvent B; 86 min, 45% solvent A, 55% solvent B. The system operated at ambient temperature. The column eluent passed through a capillary UV detector (set at 254 nm) to the MALDI sample spotter. For HILIC-MALDI-ToF/ToF Mass Spectrometry, a Probot sample fraction system (Dionex) was employed for automated spotting of the HPLC eluent onto a MALDI target at 20 s intervals. After air drying, the sample spots were overlaid with 0.5 µl 2,5-DHB matrix (1 mg ml<sup>-1</sup> in 50% aqueous methanol) and analysed by MALDI-ToF/ToF-MS on an AB-Sciex 4700. The MS spectra were obtained in automatic mode with an average 1500 laser shots/spectrum (mass range 400–2500 Da). The oligosaccharide molecular ions [M + Na]<sup>+</sup> were identified in the MALDI data and their HILIC elution positions were determined by carrying out an extracted ion chromatogram (EIC). High-energy MALDI-CID spectra were acquired with an average 10,000 laser shots/spectrum, using a high collision energy (1 kV). The oligosaccharide ions were allowed to collide in the CID cell with argon at a pressure of 2 × 10<sup>-6</sup> Torr.

#### NMR analysis

Saponified miscanthus AIR was hydrolysed with GH10 xylanase, followed by GH115 xylan glucuronidase, GH51 arabinofuranosidase and TrGH3 β-1,4-xylanase using enzyme hydrolysis conditions described above. The resulting N<sub>8</sub> oligosaccharide was then isolated by SEC as described above. Consequently, SEC fractions containing the N<sub>8</sub> oligosaccharide were pooled, solubilised in 0.6 ml D<sub>2</sub>O and analysed by NMR.

NMR spectra were recorded at 298 K with a Bruker AVANCE III spectrometer operating at 600 MHz equipped with a TCI CryoProbe. Two-dimensional <sup>1</sup>H-<sup>1</sup>H TOCSY, ROESY, <sup>13</sup>C HSQC and HSQC-TOCSY experiments were performed, using established methods [64]; the mixing times were 70 ms and 200 ms for the TOCSY and ROESY experiments, respectively. Chemical shifts were measured relative to internal acetone (δH = 2.225, δC = 31.07 ppm). Data were processed using the Azara suite of programs (v. 2.8, copyright 1993–2014, Wayne Boucher and Department of Biochemistry, University of Cambridge, unpublished) and chemical-shift assignment was performed using Analysis v2.2 [65].

#### Oligosaccharide naming system

The various hydrolysis products are named according to the Faure et al. [30] naming system. This naming system utilises a single letter code where the uppercase



letters identify the substituents of the main xylan chain. The letter “A” is attributed to single Araf substitution, the letter “U” is used for single GlcA substitution and the letter “X” for unsubstituted Xylp residues. The superscript numbers indicate substitution linkage position on Xylp. Information of side-chain modifications is included in the superscript part of the name, for example, “Me” for methylation. Finally, further substitutions of the side chains receive a new letter assignment, for example, the Araf-(1 → 2)-α-Araf-(1 → 3) side chain has been designated the “B<sup>2,3</sup>” character and the β-Xylp-(1 → 2)-α-Araf-(1 → 3) substitution has been designated the “D<sup>2,3</sup>” character [30].

### DASHBOARD software and substitution frequency quantitation

Data generated by the DNA sequencer were processed in DASHBOARD software [27] which was developed to complement the profiling technique and perform tasks such as visualisation of data, alignment of electropherograms, peak area quantification and export to Excel for further analysis.

Relative quantitation of substitution frequency was calculated after normalisation of values by comparing the abundance of side chains to the Xylp residues in the backbone. Value normalisation allowed the accurate peak area calculation by DASH software because electropherograms from higher dilution were utilised for the peak area calculation of highly abundant mono- and oligosaccharides (such as xylose and xylobiose) and the electropherograms of same samples but of lower dilution were utilised for peak area calculation of less abundant oligosaccharides. The peak area ratio between each of the xylanase oligosaccharide products and a reference oligosaccharide (XA<sup>3</sup>X and XA<sup>3</sup>XX for GH10 and GH11 digestions, respectively) resulted in the normalised values for each oligosaccharide. The total backbone Xylp present in the digested xylan was calculated as the sum of the relative quantity of each of these digestion products multiplied by the number of Xylp residues present in each structure (total backbone Xylp). For each specific side chain, side-chain substitution was calculated as the sum of the relative quantity of each of these side chains (Araf, [Me]GlcA and D<sup>2,3</sup>) multiplied by the number of side chains present in each structure (side-chain substitution). Hence, side-chain substitution frequency was calculated as the ratio between (side-chain substitution) and (total backbone Xylp).

## Additional files

**Additional file 1.** Additional figures.

**Additional file 2: Table S1.** <sup>1</sup>H and <sup>13</sup>C NMR assignments of β-Xylp-(1 → 2)-α-Araf-(1 → 3)-β-Xylp-(1 → 4)-β-Xylp-(1 → 4)-β-Xylp, at 25 °C in D<sub>2</sub>O.

### Abbreviations

DASH: DNA sequencer-Assisted Saccharide analysis in High throughput; Araf: arabinofuranose/arabinofuranosyl; Xylp: xylopyranose/xylopyranosyl; [Me] GlcA: [methyl]glucuronic acid/glucuronyl; (G)AX: (glucurono)arabinoxylan; AIR: alcohol-insoluble residue; GH: glycosyl hydrolase; GU: glucose units.

### Authors' contributions

TT designed the experimental part and carried out the analysis of xylooligosaccharides. MS and CF supported the analysis. KS performed the NMR analysis. DVR updated the DASHBOARD software. TT, NA and PD analysed the data and wrote the manuscript. All authors read and approved the final manuscript.

### Author details

<sup>1</sup> Department of Biochemistry, University of Cambridge, Hopkins Building, The Downing Site, Tennis Court Road, Cambridge CB2 1QW, UK. <sup>2</sup> Department of Biochemistry, University of Cambridge, Sanger Building, 80 Tennis Court Road, Cambridge CB2 1GA, UK. <sup>3</sup> Present Address: Scion, 49 Sala Street, Private Bag 3020, Rotorua 3046, New Zealand. <sup>4</sup> Present Address: Frontiers, WeWork, 1 Fore St, London EC2Y 5EJ, UK. <sup>5</sup> Present Address: ideaSpace South, Cambridge Biomedical Campus, Bay 13 Hills Road, Cambridge CB2 0SP, UK.

### Acknowledgements

We thank Dr. Tina Theys and Dr. Rita Marques for technical support.

### Competing interests

The authors declare that they have no competing interests.

### Availability of data and materials

The dataset supporting the conclusions of this article is included within the article and its additional files.

### Consent for publication

All authors read and approved the final manuscript.

### Ethics approval and consent to participate

Not applicable.

### Funding

The work was funded by the BBSRC (BSBEC BIOMASS BB/G016216/1 and BB/K005537/1) and the European Community's Seventh Framework Programme SUNLIBB (FP7/2007–2013) under the Grant Agreement No. 251132 to P.D. The Cambridge NMR facility infrastructure is funded by the BBSRC and the Wellcome Trust. We are grateful for plant material from Aberystwyth, Rothamsted and Wageningen University, NL.

## Publisher's Note

Springer Nature remains neutral with regard to jurisdictional claims in published maps and institutional affiliations.

Received: 2 January 2019 Accepted: 25 April 2019

Published online: 06 May 2019

## References

- Ebringerová A, Heinze T. Xylan and xylan derivatives—biopolymers with valuable properties, 1. Naturally occurring xylans structures, isolation procedures and properties. *Macromol Rapid Commun.* 2000;21:542–56.
- Saulnier L, Vigouroux J, Thibault J-F. Isolation and partial characterization of feruloylated oligosaccharides from maize bran. *Carbohydr Res.* 1995;272(2):241–53.

3. Tian L, Gruppen H, Schols HA. Characterization of (Glucurono)arabinoxylans from oats using enzymatic fingerprinting. *J Agric Food Chem*. 2015;63(50):10822–30.
4. Hatfield RD, Rancour DM, Marita JM. Grass cell walls: a story of cross-linking. *Front Plant Sci*. 2017;7:2056.
5. Mueller-Harvey I, Hartley RD, Harris PJ, Curzon EH. Linkage of *p*-coumaroyl and feruloyl groups to cell-wall polysaccharides of barley straw. *Carbohydr Res*. 1986;148(1):71–85.
6. de Buanafina OMM. Feruloylation in grasses: current and future perspectives. *Mol Plant*. 2009;2(5):861–872.
7. Ishii T. Structure and functions of feruloylated polysaccharides. *Plant Sci*. 1997;127(2):111–27.
8. Wende G, Fry SC. 2-O- $\beta$ -D-xylopyranosyl-(5-O-feruloyl)-L-arabinose, a widespread component of grass cell walls. *Phytochemistry*. 1997;44(6):1019–30.
9. Chiniquy D, Sharma V, Schultink A, Baidoo EE, Rautengarten C, Cheng K, Carroll A, Ulvskov P, Harholt J, Keasling JD, et al. XAX1 from glycosyltransferase family 61 mediates xylosyltransfer to rice xylan. *Proc Natl Acad Sci USA*. 2012;109(42):17117–22.
10. Appeldoorn MM, de Waard P, Kabel MA, Gruppen H, Schols HA. Enzyme resistant feruloylated xylooligomer analogues from thermochemically treated corn fiber contain large side chains, ethyl glycosides and novel sites of acetylation. *Carbohydr Res*. 2013;381:33–42.
11. Allerdings E, Ralph J, Steinhart H, Bunzel M. Isolation and structural identification of complex feruloylated heteroxylan side-chains from maize bran. *Phytochemistry*. 2006;67(12):1276–86.
12. Appeldoorn MM, Kabel MA, Van Eylen D, Gruppen H, Schols HA. Characterization of oligomeric xylan structures from corn fiber resistant to pretreatment and simultaneous saccharification and fermentation. *J Agric Food Chem*. 2010;58(21):11294–301.
13. Coelho E, Rocha MAM, Moreira ASP, Domingues MRM, Coimbra MA. Revisiting the structural features of arabinoxylans from brewers' spent grain. *Carbohydr Polymers*. 2016;139:167–76.
14. Schendel RR, Meyer MR, Bunzel M. Quantitative profiling of feruloylated arabinoxylan side-chains from graminaceous cell walls. *Front Plant Sci*. 2016;6:1249.
15. Ishii T. Acetylation at O-2 of arabinofuranose residues in feruloylated arabinoxylan from bamboo shoot cell-walls. *Phytochemistry*. 1991;30(7):2317–20.
16. McCann MC, Carpita NC. Designing the deconstruction of plant cell walls. *Curr Opin Plant Biol*. 2008;11(3):314–20.
17. Simmons TJ, Mortimer JC, Bernardinelli OD, Pöppler A-C, Brown SP, deAzevedo ER, Dupree R, Dupree P. Folding of xylan onto cellulose fibrils in plant cell walls revealed by solid-state NMR. *Nat Commun*. 2016;7:13902.
18. DeMartini JD, Pattathil S, Miller JS, Li HJ, Hahn MG, Wyman CE. Investigating plant cell wall components that affect biomass recalcitrance in poplar and switchgrass. *Energy Environ Sci*. 2013;6(3):898–909.
19. Hojje A, Sandstrom C, Roubroeks JP, Andersson R, Gohil S, Gatenholm P. Evidence of the presence of 2-O- $\beta$ -D-xylopyranosyl- $\alpha$ -L-arabinofuranose side chains in barley husk arabinoxylan. *Carbohydr Res*. 2006;341(18):2959–66.
20. Marcotuli I, Hsieh YSY, Lahnstein J, Yap K, Burton RA, Blanco A, Fincher GB, Gadaleta A. Structural variation and content of arabinoxylans in endosperm and bran of durum wheat (*Triticum turgidum* L.). *J Agric Food Chem*. 2016;64(14):2883–92.
21. Pastell H, Virkki L, Harju E, Tuomainen P, Tenkanen M. Presence of  $\alpha$ -linked 2-O- $\beta$ -D-xylopyranosyl- $\alpha$ -L-arabinofuranosyl side chains in cereal arabinoxylans. *Carbohydr Res*. 2009;344(18):2480–8.
22. Toole G, Wilson R, Parker M, Wellner N, Wheeler T, Shewry P, Mills E. The effect of environment on endosperm cell-wall development in *Triticum aestivum* during grain filling: an infrared spectroscopic imaging study. *Planta*. 2007;225(6):1393–403.
23. Ordaz-Ortiz JJ, Devaux M-F, Saulnier L. Classification of wheat varieties based on structural features of arabinoxylans as revealed by endoxylanase treatment of flour and grain. *J Agric Food Chem*. 2005;53(21):8349–56.
24. Bowman MJ, Dien BS, Vermillion KE, Mertens JA. Structural characterization of (1  $\rightarrow$  2)- $\beta$ -xylose-(1  $\rightarrow$  3)- $\alpha$ -arabinose-containing oligosaccharide products of extracted switchgrass (*Panicum virgatum*, L.) xylan after exhaustive enzymatic treatment with  $\alpha$ -arabinofuranosidase and  $\beta$ -endo-xylanase. *Carbohydr Res*. 2014;398:63–71.
25. Kulkarni A, Pena MJ, Avci U, Mazumder K, Urbanowicz B, Pattathil S, Yin Y, O'Neill MA, Roberts AW, Hahn MG, et al. The ability of land plants to synthesize glucuronoxylans predates the evolution of tracheophytes. *Glycobiology*. 2011;22(3):1–15.
26. Peña MJ, Kulkarni AR, Backe J, Boyd M, O'Neill MA, York WS. Structural diversity of xylans in the cell walls of monocots. *Planta*. 2016;244(3):589–606.
27. Li X, Jackson P, Rubtsov D, Faria-Blanc N, Mortimer J, Turner S, Krogh K, Johansen K, Dupree P. Development and application of a high throughput carbohydrate profiling technique for analyzing plant cell wall polysaccharides and carbohydrate active enzymes. *Biotechnol Biofuels*. 2013;6(1):94.
28. Biely P, Vrsanská M, Tenkanen M, Kluepfel D. Endo-[beta]-1,4-xylanase families: differences in catalytic properties. *J Biotechnol*. 1997;57(1–3):151–66.
29. Maslen SL, Goubet F, Adam A, Dupree P, Stephens E. Structure elucidation of arabinoxylan isomers by normal phase HPLC-MALDI-TOF/TOF-MS/MS. *Carbohydr Res*. 2007;342(5):724–35.
30. Faure R, Courtin CM, Delcour JA, Dumon C, Faulds CB, Fincher GB, Fort S, Fry SC, Halila S, Kabel MA, et al. A brief and informationally rich naming system for oligosaccharide motifs of heteroxylans found in plant cell walls. *Aust J Chem*. 2009;62(6):533–7.
31. Guile GR, Rudd PM, Wing DR, Prime SB, Dwek RA. A rapid high-resolution high-performance liquid chromatographic method for separating glycan mixtures and analyzing oligosaccharide profiles. *Anal Biochem*. 1996;240(2):210–26.
32. Domon B, Costello CE. A systematic nomenclature for carbohydrate fragmentations in FAB-MS/MS spectra of glycoconjugates. *Glycoconj J*. 1988;5(4):397–409.
33. Chai W, Piskarev V, Lawson AM. Negative-ion electrospray mass spectrometry of neutral underivatized oligosaccharides. *Anal Chem*. 2001;73(3):651–7.
34. Bromley JR, Busse-Wicher M, Tryfona T, Mortimer JC, Zhang Z, Brown DM, Dupree P. GUX1 and GUX2 glucuronyltransferases decorate distinct domains of glucuronoxylan with different substitution patterns. *Plant J*. 2013;74(3):423–34.
35. Spina E, Sturiale L, Romeo D, Impallomeni G, Garozzo D, Waidelich D, Glueckmann M. New fragmentation mechanisms in matrix-assisted laser desorption/ionization time-of-flight/time-of-flight tandem mass spectrometry of carbohydrates. *Rapid Commun Mass Spectrom*. 2004;18(4):392–8.
36. Beylot MH, Emami K, McKie VA, Gilbert HJ, Pell G. *Pseudomonas cellulosa* expresses a single membrane-bound glycoside hydrolase family 51 arabinofuranosidase. *Biochem J*. 2001;358(3):599–605.
37. Nurizzo D, Nagy T, Gilbert HJ, Davies GJ. The structural basis for catalysis and specificity of the *Pseudomonas cellulosa*  $\alpha$ -glucuronidase, GlcA67A. *Structure*. 2002;10(4):547–56.
38. Rogowski A, Basle A, Farinas CS, Solovyova A, Mortimer JC, Dupree P, Gilbert HJ, Bolam DN. Evidence that GH115  $\alpha$ -glucuronidase activity, which is required to degrade plant biomass, is dependent on conformational flexibility. *J Biol Chem*. 2014;289(1):53–64.
39. Thibault J-F. Separation of  $\alpha$ -D-galacturonic acid oligomers by chromatography on polyacrylamide gel. *J Chromatogr A*. 1980;194(3):315–22.
40. Himmelsbach D, Hartley RD, Borneman W, Poppe L, Van Halbeek H. Structure of a feruloylated arabinoxylan tetrasaccharide that contains the  $\beta$ -D-Xylp-(1  $\rightarrow$  2)- $\alpha$ -L-Araf element by <sup>1</sup>H and <sup>13</sup>C NMR spectroscopy. *Magn Reson Chem*. 1994;32(3):158–65.
41. Moller I, Marcus SE, Haeger A, Verherbruggen Y, Verhoef R, Schols H, Ulvskov P, Mikkelsen D Jr, Knox JP, Willats W. High-throughput screening of monoclonal antibodies against plant cell wall glycans by hierarchical clustering of their carbohydrate microarray binding profiles. *Glycoconjugate J*. 2008;25(1):37–48.
42. da Costa RM, Pattathil S, Avci U, Lee SJ, Hazen SP, Winters A, Hahn MG, Bosch M. A cell wall reference profile for *Miscanthus* bioenergy crops highlights compositional and structural variations associated with development and organ origin. *New Phytol*. 2017;213(4):1710–25.
43. Badhan A, Wang Y, McAllister TA. Analysis of complex carbohydrate composition in plant cell wall using Fourier Transformed Mid-Infrared Spectroscopy (FT-IR). In: Abbott DW, van Lammerts Bueren A, editors.

- Protein-carbohydrate interactions: methods and protocols. New York: Springer; 2017. p. 209–14.
44. Robert P, Marquis M, Barron C, Guillon F, Saulnier L. FT-IR investigation of cell wall polysaccharides from cereal grains. *Arabinoxylan infrared assignment*. *J Agric Food Chem*. 2005;53(18):7014–8.
  45. Sun X-F, Sun RC, Fowler P, Baird MS. Extraction and characterization of original lignin and hemicelluloses from wheat straw. *J Agric Food Chem*. 2005;53(4):860–70.
  46. Bengtsson S, Aman P, Andersson RE. Structural studies on water-soluble arabinoxylans in rye grain using enzymatic hydrolysis. *Carbohydr Polymers*. 1992;17(4):277–84.
  47. Gruppen H, Kormelink FJM, Voragen AGJ. Water-unextractable cell wall material from wheat flour. 3. A structural model for arabinoxylans. *J Cereal Sci*. 1993;18(2):111–28.
  48. Verbruggen MA, Beldman G, Voragen AGJ. Enzymic degradation of sorghum glucuronoarabinoxylans leading to tentative structures. *Carbohydr Res*. 1998;306(1–2):275–82.
  49. Pena MJ, Kulkarni AR, Backe J, Boyd M, O'Neill MA, York WS. Structural diversity of xylans in the cell walls of monocots. *Planta*. 2016;244:589–606.
  50. Kulkarni A, Pattathil S, Hahn MG, York WS, O'Neill MA. Comparison of arabinoxylan structure in bioenergy and model grasses. *Ind Biotechnol*. 2012;8(4):222–9.
  51. Xiao C, Zhang T, Zheng Y, Cosgrove DJ, Anderson CT. Xyloglucan deficiency disrupts microtubule stability and cellulose biosynthesis in *Arabidopsis*, altering cell growth and morphogenesis. *Plant Physiol*. 2015;170(1):234–49.
  52. da Costa RMF, Lee SJ, Allison GG, Hazen SP, Winters A, Bosch M. Genotype, development and tissue-derived variation of cell-wall properties in the lignocellulosic energy crop *Miscanthus*. *Ann Bot*. 2014;114(6):1265–77.
  53. Verbruggen MA, Spronk BA, Schols HA, Beldman G, Voragen AGJ, Thomas JR, Kamerling JP, Vliegthart JFG. Structures of enzymically derived oligosaccharides from sorghum glucuronoarabinoxylan. *Carbohydr Res*. 1998;306(1):265–74.
  54. Mazumder K, York WS. Structural analysis of arabinoxylans isolated from ball-milled switchgrass biomass. *Carbohydr Res*. 2010;345(15):2183–93.
  55. Charnock SJ, Spurway TD, Xie H, Beylot M-H, Virden R, Warren RAJ, Hazlewood GP, Gilbert HJ. The topology of the substrate binding clefts of glycosyl hydrolase family 10 xylanases are not conserved. *J Biol Chem*. 1998;273(48):32187–99.
  56. Gilbert HJ, Hazlewood GP, Laurie JI, Orpin CG, Xue GP. Homologous catalytic domains in a rumen fungal xylanase: evidence for gene duplication and prokaryotic origin. *Mol Microbiol*. 1992;6(15):2065–72.
  57. Nagy T, Nurizzo D, Davies GJ, Biely P, Lakey JH, Bolam DN, Gilbert HJ. The  $\alpha$ -glucuronidase, GlcA67A, of *Cellvibrio japonicus* utilizes the carboxylate and methyl groups of aldobiouronic acid as important substrate recognition determinants. *J Biol Chem*. 2003;278(22):20286–92.
  58. Ryabova O, Vrřanská M, Kaneko S, van Zyl WH, Biely P. A novel family of hemicellulolytic  $\alpha$ -glucuronidase. *FEBS Lett*. 2009;583(9):1457–62.
  59. Peng W, Pedersen NR, Pettersson D, Ekloff JM, Nyman-Garup S, Palmén LG, Monrad RN, Spodsberg N, Stringer MA, Blom C et al. Compositions comprising polypeptides having xylanase activity and polypeptides having arabinofuranosidase activity. 2017. US 2017/0335302 A1.
  60. Margolles-Clark E, Tenkanen M, Nakari-Setälä T, Penttilä M. Cloning of genes encoding  $\alpha$ -L-arabinofuranosidase and  $\beta$ -xylosidase from *Trichoderma reesei* by expression in *Saccharomyces cerevisiae*. *Appl Environ Microbiol*. 1996;62(10):3840–6.
  61. Goubet F, Jackson P, Deery MJ, Dupree P. Polysaccharide analysis using carbohydrate gel electrophoresis: a method to study plant cell wall polysaccharides and polysaccharide hydrolases. *Anal Biochem*. 2002;300(1):53–68.
  62. Tryfona T, Theys TE, Wagner T, Stott K, Keegstra K, Dupree P. Characterisation of FUT4 and FUT6  $\beta$ -(1  $\rightarrow$  2)-fucosyltransferases reveals that absence of root arabinogalactan fucosylation increases *Arabidopsis* root growth salt sensitivity. *PLoS ONE*. 2014;9(3):e93291.
  63. Tryfona T, Stephens E. Analysis of carbohydrates on proteins by offline normal-phase liquid chromatography MALDI-ToF/ToF-MS/MS. *Meth Mol Biol*. 2010;658(2):137–51.
  64. Cavanagh J, Fairbrother WJ, Palmer AG, Skelton NJ. *Protein NMR spectroscopy: principles and practice*. San Diego: Academic Press; 1996.
  65. Vranken WF, Boucher W, Stevens TJ, Fogh RH, Pajon A, Llinas M, Ulrich EL, Markley JL, Ionides J, Laue ED. The CCPN data model for NMR spectroscopy: development of a software pipeline. *Proteins Struct Funct Bioinform*. 2005;59(4):687–96.

Ready to submit your research? Choose BMC and benefit from:

- fast, convenient online submission
- thorough peer review by experienced researchers in your field
- rapid publication on acceptance
- support for research data, including large and complex data types
- gold Open Access which fosters wider collaboration and increased citations
- maximum visibility for your research: over 100M website views per year

At BMC, research is always in progress.

Learn more [biomedcentral.com/submissions](https://biomedcentral.com/submissions)

